Zeeden, C., Ulfers, A., Pierdominici, S., Abadi, M. S., Vinnepand, M., Grelle, T., Hesse, K., Leu, K., Wonik, T. (2023): Downhole logging data for time series analysis and cyclostratigraphy. - Earth-Science Reviews, 241, 104436.

https://doi.org/10.1016/j.earscirev.2023.104436

# Downhole logging data for time series analysis and cyclostratigraphy

Christian Zeeden[a,*], Arne Ulfers[a, b], Simona Pierdominici[c], Mehrdad Sardar Abadi[a], Mathias Vinnepand[a], Thomas Grelle[a], Katja Hesse[a, d], Katharina Leu[a], Thomas Wonik[a,*]

[a] LIAG, Leibniz Institute for Applied Geophysics, Stilleweg 2, 30655 Hannover, Germany

[b] BGR, Federal Institute for Geosciences and Natural Resources, Stilleweg 2, 30655 Hannover, Germany

[c] Helmholtz-Centre Potsdam, German Research Centre for Geosciences – GFZ, Telegrafenberg, 14473, Potsdam, Germany

[d] Georg-August-Universität Göttingen, Goldschmidtstraße 3, 37077 Göttingen

* corresponding author: christian.zeeden@leibniz-liag.de

Key words: downhole logging; cyclostratigraphy; astrochronology; time series analysis;

**Abstract**

Numerous borehole logging datasets gathered for commercial and scientific purposes are available around the globe. However, studies valorising the chronostratigraphic potential of these datasets through time series analyses remain sparse despite the excellent completeness of downhole logging data retrieved in a fast and high-resolution fashion. The major reason for this is the complexity of such approaches and potential pitfalls that may discourage non-experienced users. Here we provide an overview that summarizes the most relevant properties of borehole logging measurements for time series analysis and cyclostratigraphy. Further, we provide a brief introduction of most relevant time series analyses methods, including several examples of borehole logging cyclostratigraphy. Compared to analyses and interpretations of data from cores or exposures, it is important to be aware of borehole logging data specific pitfalls. These include environmental corrections like the effect of variation in borehole diameter, the effects of drilling fluids, and that presented logs may consist of merged results logged in several depth sections.

## 1. Introduction

Borehole logging, also known as well-, wireline- or downhole logging, is the practice of measuring the physical, chemical, and structural properties of the drilled geological underground using geophysical tools that are lowered into a borehole on a wireline cable (e.g., Pierdominici and Kück, 2021; Rider and Kennedy, 2011). In this contribution, we focus on conventional downhole logging measurements acquired in semi vertical boreholes, though similar datasets may be acquired through logging-while-drilling and logging-while-tripping.

Downhole logging data provide a continuous record that delivers in-situ information on the sedimentologcial/lithological properties and changes with a precision of commonly decimetres to few centimetres. These include the physical properties of the strata and possibly contained fluids (Wilke et al., 2016). Through investigating petrophysical characteristics as a function of depth, downhole logging is frequently used in combination with seismic reflection data to create geological models. In addition, the combination of downhole logging data and petrophysical datasets from drill cores are often essential to construct a composite of core depths (e.g., Shackleton et al., 1999; Wilke et al., 2016), especially where cores are either incomplete or expanded due to decompaction. Application of time series analysis, cyclostratigraphy, and derivation of paleoclimate and paleoceanographic information (e.g., Bahk et al., 2016) from borehole logging data are not a recent development (e.g., Fischer and Roberts, 1991; Goldhammer et al., 1994; Huang et al., 2010; Weedon et al., 2004, 1999; Yang and Baumfalk, 1994), but we see an increase in such applications. Because time series analyses are mostly carried out in sediments with the aim of understanding climate-related signals, we focus on such applications on Milankovitch time scale here (and not on very short quasi-cycles as e.g., warves, and not on cyclic systems of non-climatic origin as e.g. tidal rhythmites).

### 1.1. Time series, time series analyses and astrochronology in Earth sciences

#### 1.1.1. Geological time series are commonly depth series

The term "geological time series" means geological depth series that represent time. These can be determined in an exposure, a drill core, or derive from borehole logging data (Figs. 1 and 2). Stratigraphic depth is related to deposition time, and accumulation/sedimentation rates commonly vary in complex ways (Weedon, 2003). Such depth series may be brought onto a geological time scale in different manners, but these time scales will never perfectly represent time (though layer-counted archives with annual resolution, varves, come close allowing for missing laminae and occasional multiple laminae in a year) due to changing sedimentation rates and a limited amount of unambiguous points in depth for which time is known with little uncertainty. This means that while sampling may be uniform in depth, the same sampling may be highly inconsistent in time. In addition, gaps in sedimentation or layers with immediate deposition in the form of slumps or volcanic deposits may be present in a stratigraphic sequence. To eliminate the extreme variations in sedimentation rate implied, such instantaneously-deposited layers need to be removed from stratigraphies for time series analyses (Fig. 3).

### 1.1.2. Translating stratigraphy to time

Sediments represent series of deposition over time. The continuity, homogeneity and sedimentation rate depends on the sedimentary system and on the considered scale. Generally, systems which have a quasi-continuous sedimentation over 'long' or relevant time spans are natural targets for time series analyses. The more uniform sedimentation rates are, the better. Such milieus typically prevail e.g. in the (deep) ocean and in large lakes.

The construction of geological time series from stratigraphical depth series may be achieved through a set of direct dates and interpolation or modelling in between these (e.g., De Vleeschouwer and Parnell, 2014; Telford et al., 2004; Trachsel and Telford, 2017; Zeeden et al., 2018a). Further, layer counting can give precise ages between such dated positions (e.g., Czymzik et al., 2015; Obreht et al., 2020). In astrochronology, not layers but the intricate patterns of eccentricity, obliquity and precession are used (either together or individually) to obtain information on the relative timing in a stratigraphic succession (e.g., Hilgen et al., 2015; Hinnov, 2000; Hinnov and Hilgen, 2012). Also this astrochronologic non-exact information on the duration between dated layers is used in combination with dated layers (e.g., De Vleeschouwer and Parnell, 2014; Meyers et al., 2012; Rivera et al., 2011).

Note that an equally spaced sampling in depth will result in a non-uniform sampling rate once the stratigraphic domain is translated into a time domain. Therefore, a higher-than-necessary sampling resolution in depth is generally advised, as shown in a modelling study by Martinez et al., (2016).

When applying any methods transferring geological depth to age, experienced earth scientists check typical sedimentation rates for the respective depositional system, and the change in sedimentation itself against the model outcome. Rapid changes in sedimentation rate may be considered suspicious and the result of over-tuning data. Ideally, an integrated stratigraphical approach relying on information from several dating methods should be applied, where astrochronology may provide the highest resolution (Hilgen et al., 2015).

### 1.1.3. Astrochronology with emphasis on application to borehole logging data

Understanding the reaction of Earth's system to astronomical and orbital insolation forcing is a relevant aspect for several disciplines in Earth sciences. The reaction of the climate system to insolation is clearly complex (e.g., Friedrich et al., 2016; Hagelberg and Pisias, 1990; Liebrand et al., 2017; Meyers, 2019; Yi et al., 2017), and also sedimentary systems react to this forcing in complex ways (e.g., Fischer et al., 1991; Hüsing et al., 2009; Vaucher et al., 2021). One may ask the question if any sedimentary system is unaffected by changing insolation. The need to understand the response of climate and sedimentary systems to quasi-cyclic variations in insolation (Laskar et al., 2004; Milankovitch, 1941) led to a suite of time series analysis techniques being applied and developed for this purpose (e.g., Meyers, 2019 and references therein). Most published data related to paleoclimate originate from exposures and drill cores (e.g., Cheddadi and Rossignol-Strick, 1995; Colman et al., 1995; Hodell and Channell, 2016; Kaboth-Bahr et al., 2020; Liebrand et al., 2017; Martinez et al., 2013; Trauth et al., 2009; Vinnepand et al., 2022; Yang and Ding, 2014), among others from the International Ocean Discovery Program (IODP) and the International Continental Scientific Drilling Program (ICDP) campaigns. However, additionally borehole logging data contributes valuable data for understanding Earth history (Figs. 3, 4; e.g., Baumgarten et al., 2015; Fischer and Roberts, 1991; Goldhammer et al., 1994; Li et al., 2019b; Morgans-Bell et al., 2001; Read et al., 2020; Sierro et al., 2000; Ulfers et al., 2021, 2022b).

### 1.2. Borehole logging data in comparison to core data

In the industry the main reason for generating borehole logging data is the efficient recovery of hydrocarbons and other resources. In contrast, applications of borehole logging have become more important and diversified since the 1990s in earth sciences. Worthington (1990) discusses the potential and resolution limits of borehole logging data and suitability for detecting astronomical climate forcing in logging data. Among others, Fischer (1995) suggests "combining geophysical, geochemical and geobiological data" in the context of logging data and cyclostratigraphy. Early users of logging data for cyclostratigraphy include (Molinie and Ogg, 1990; Shackleton et al., 1999). Shackleton et al., (1999) used well logging data to tie core-and log data together and established a stratigraphy and time frame for Oligocene-Miocene parts of ODP Leg 154 sites from the Ceará Rise in the western equatorial Atlantic. Several successful and valuable cyclostratigraphic analyses of downhole logging data from sedimentary sequences (e.g., Baumgarten et al., 2015; Shackleton et al., 1999; Voigt et al., 2008; Wonik, 2001) have brought logging data more and more into the awareness of cyclostratigraphers. One reason for this is the uninterrupted length over 10s to 1000s of metres of high resolution (decimentres to centimetres) logging data that renders them advantageous, compared to core data. The latter may not comprise a complete stratigraphy (due to core loss) and may be biased through effects caused by drilling and recovery procedures.

Further, the fast availability of logging data during, or directly after the operations allows for valuable first impressions of sedimentary structures including the (non)presence of quasi-cyclic alterations (commonly before cores are opened). In addition, it is generally accepted that logging data have a good depth scale, which can be used to bring core material and physical properties thereof onto the same most accurate logging-derived depth scale (e.g., Morgans-Bell et al., 2001; Weedon, 2003). Depth for cores is often more challenging to determine in detail due to factors such as core loss and decompaction of soft sediment.

Downhole logging data may not always have the depth- and temporal- resolution to reconstruct all relevant sedimentary cycles (Worthington, 1990) e.g. they may allow the detection of ~100 kyr eccentricity cycles, but not the shorter ~20 kyr precession cycles. Care must be taken to have sufficient sampling and data resolution (Martinez et al., 2016).

An increasing suite of studies applies cyclostratigraphy and time series analysis to downhole logging datasets (e.g., Baumgarten et al., 2015; Giaccio et al., 2019; Nowaczyk, 2001; Radzevičius et al., 2014; Read et al., 2020; Sierro et al., 2000; Ulfers et al., 2021; Worthington, 1990), not always describing and discussing the dataset's origin and acquisition in detail. This may not be an issue, but we generally consider it relevant to be aware of possible shortcomings. Here, we summarize most relevant properties of logging data for geological time series analysis and cyclostratigraphy.

## 2. Specific properties of borehole logging data: chances and challenges

This section describes aspects of downhole logging practise, with a special focus on relevant information that allow critical assessment of the quality of resulting data. The borehole itself, and its properties directly influences logging results. In this context, drilling fluids can enter the sediment in different amounts depending on the fluid and rock properties, affecting logging measurements. For example, intrusion of a clay-rich drilling fluid into a quartz sandstone will lead to higher magnetic susceptibility and lower porosity. The shape of the borehole wall (caliper) can be of importance, and is dependent on lithology, e.g., with little wider diameters in unconsolidated layers (Fig. 1). Further, the borehole shape can be influenced by the stress field and the fracture intensity. Connecting parts of the drill string may influence the borehole wall, and possibly induce an artificial cyclic pattern through equally spaced larger borehole diameters around these pipe connectors.

### 2.1. Downhole logging on site

Downhole logging operations start during drilling breaks or when the drilling of a hole is finished. Depending on the borehole properties, logging may be performed in an open hole or through a casing. Plastic casings are not an issue for geophysical methods based on gamma radiation, and electromagnetic properties as the magnetic susceptibility and induction/conductivity and seismic properties. Conversely, metal casings effectively prevent most tools from being useful (with exceptions of gamma ray measurements, salinity, temperature and seismic velocity investigations). In practice, not all logging probes can be tied to a single logging string, and different tools may acquire data during consecutive logging runs. Depth-synchronization can then be achieved through adding the same sensor(s) to all logging runs (often a gamma ray probe). However, despite this, logging datasets from multiple tools may not be perfectly depth-synchronized. In this context, depth differences can be expected to be small, but may be relevant for consecutive (multivariate) statistical analysis. Because only few boreholes remain open and accessible after drilling campaigns, data acquired on-site sometimes constitute the only possible continuous dataset to retrieve. Therefore, careful planning of which measurements to apply, and which resolution and logging speed to implement is essential. The logging speed depends on the used tools/sensors, and together with the sampling interval influences on the data quality. Typical logging speeds are between 60 m/h and 600 m/h (Wilke et al., 2016), but reduced logging speed can be useful for highest-resolution logging.

Continuous datasets can often be generated, but sometimes logging takes place for different depth intervals individually as drilling pipes are being tripped out in steps to ensure an open hole. In these cases, logging datasets actually represent composite records – often but not always with overlap (Fig. 2; e.g., Baumgarten et al., 2014; Ulfers et al., 2021).

### 2.2. Technical aspects

Borehole logging records data in the sediment/rock unit itself (in-situ) and is not prone to issues of decompaction and core loss. This means that borehole logging data provide more reliable depth information than core data, but may have less depth resolution than data obtained through high-resolution core scanning. The vertical and radial extent of an investigated volume investigated through downhole logging tools is influenced by several factors including the borehole diameter, the properties of the borehole including fluids (mud weight), the position of the tool in the borehole (e.g. centralized or decentralized), and the design of the tool itself (detector size, transmitter-receiver spacing, volume of influence). Thus, each tool has a characteristic depth resolution and an average radial area of investigation at specific conditions (Wilke et al., 2016). The advantage of in-situ measurements may be counteracted by the effects of drilling fluids or cementations that affect the signal of especially porous rocks. Boreholes commonly do not have a perfectly constant diameter, but caliper measurements may be used to assess comparability and correct for changing diameters (e.g., Lehmann, 2010, and references therein). The content of drilling fluids, drill pipes, casing, and infill between a casing and the borehole wall affect logging data. Thick metal casing will attenuate gamma ray signals. Also any infill between borehole wall and casing will influence logging properties, e.g. a clay-rich infill may lead to higher gamma ray signals and suggest more clay-rich strata than is actually present. A suite of correction methods has been compiled for different logging conditions. Several models and concepts can be applied to eliminate biases (e.g. chartbooks: Schlumberger, 2013; Weatherford, 2007). The effects of tool joints within the drill string or casing can change logging results and need to be considered (e.g., Lehmann, 2010).

### 2.3. Selected physical properties

A large suite of relevant physical and chemical parameters can be measured using logging devices. Rider and Kennedy (2011) provide a good overview on this topic (see also table 1 for parameters and their applications in cyclostratigraphy). Here, we focus on parameters which commonly reflect changes in the paleo-environment and are therefore sedimentologically meaningful, and which have a rather high vertical depth resolution, making them especially useful for geological time series analysis and the detection of high frequency oscillations in the record. However, care must be taken not to over-interpret the resolution of logging datasets (Worthington, 1990), because the reported data resolution may be higher than the actual resolution between two independent measurements due to sensor properties. Some logging sensors require a longer than preferred depth interval (cm-m) and do not provide fully independent data points with high depth resolution. While higher data resolution (= sample rates) can be achieved, such data are commonly smoothed and integrate a longer depth interval (and large 3-dimensional volume) than the sampling rate may suggest. The best way to obtain high resolution data is a combination of a high sampling rate and a slow run of logging tools. Although deconvolution based on the tools' properties may help to increase resolution, such mathematical procedures are often not applied in order to avoid the introduction of artefacts.

In the following sections, we focus on most relevant downhole logging methods, although other logging datasets may be useful for cyclostratigraphy. Yet, their depth resolution is generally lower, and therefore high sedimentation rates are required for obtaining a good signal also of high frequency components. As we aim to provide an overview, we refrain from discussing existing special lithologies, where an uncommon sedimentology may require different interpretations.

#### 2.3.1. Gamma radiation logging

A record of gamma ray (GR) emission in sediments reflects the presence of naturally occurring radiogenic elements. Radiogenic isotopes of the elements potassium ($^{40}$K), uranium ($^{238}$U), and thorium ($^{232}$Th) are the dominant sources of gamma rays in sedimentary rocks (see Fig. 5; e.g., Ruffell and Worden, 2000). The spatial and temporal distribution of radiogenic elements in sedimentary sequences may reflect multiple sources of sediments, as well as various environmental conditions affecting sedimentary materials before and after sedimentation (e.g., Sardar Abadi et al., 2022).

While K is commonly associated with feldspars, micas, and clays, U may be concentrated in organic-rich intervals (redox processes), but is also part of some heavy minerals and may be bound to clay. The Th content may be associated with clays and volcanic ash layers. Because the spectral gamma ray (SGR) components are related to K, U, and Th, also element ratios are interpreted (e.g., Hunze et al., 2013; Ruffell and Worden, 2000; Schnyder et al., 2006). Therefore, the Th/U ratio may help to detect ash layers (Li et al., 2019b; Ruffell and Worden, 2000). Due to its clear relation to lithology, GR is commonly used for correlation between logs, cores and for core-log integration (Lofi et al., 2016). Yet, magnetic susceptibility sondes allow for higher resolution signal acquisition, and are therefore preferred where this variable is a useful proxy (Weedon et al., 1999).

Relatively high GR data are often associated with the terrestrial clastic influx of clay and coarser materials, while relatively low GR values may correspond to sedimentation of biogenic carbonate, organic carbon, or silica (e.g., Rider and Kennedy, 2011) both in lacustrine and marine environments. However, the combination of other proxies from downhole logging data such as magnetic susceptibility can help in defining the detrital origin of GR signals.

GR can be logged in pipes and through drill strings, although these dampen the signal. In such cases, care needs to be advised not to interpret the high attenuation effect of logging pipe connectors as a quasi-cyclic signal.

An example showing the paleo-environmental relationship of GR is the sediment succession of the 1.36 million year old Lake Ohrid in North Macedonia/Albania (Fig. 4, Wagner et al., 2014). During interglacials, the supply and deposition of carbonates is enhanced due to an active karst system. In glacials, when the karst system is less active, the relative proportion of terrestrial clastic input is increased. The periodic alternation between high GR values in cold periods and low GR values in the carbonate-rich sediments of warmer periods is well established in the downhole records of Lake Ohrid (Alexander Francke et al., 2016; Ulfers et al., 2022b; Vogel et al., 2010).

GR data from offshore drilling in Portugal related to the Mediterranean outflow and associated contourites have been found to be driven by a combination of several impacting factors (Lofi et al., 2016). Terrestrial influx of clay minerals is driven by glacial/interglacial sea level changes with low sea level providing more terrestrial flux (higher GR). Also precession-driven runoff from the Iberian Peninsula provides clay minerals and enhances GR in phases of high insolation. Further, sandy contourite beds (low GR) are related to Mediterranean outflow dynamics and represent arid and low insolation phases (Lofi et al., 2016).

Also because of the mostly straightforward interpretation of GR logs, these are commonly used targets for astrochronology (e.g., Baumgarten et al., 2015; Huang et al., 2020; Liu et al., 2020, 2001; Lofi et al., 2016; Ochoa et al., 2018, 2015; Read et al., 2020; Ruffell and Worden, 2000; Ulfers et al., 2022b; Wonik, 2001; Table 1).

### 2.3.2. Magnetic susceptibility logging

The magnetic susceptibility (MS) is defined as the reaction of a sample to an applied (alternating) magnetic field. It can easily be measured in the field, in the laboratory and also using well logging tools. Minerals can be divided into those having ferromagnetic, paramagnetic and diamagnetic properties. Ferromagnetic minerals as e.g., magnetite can store magnetic field properties. Magnetite has a naturally high MS, and often dominates magnetic signatures even if present in small quantities. Hematite and goethite are also ferromagnetic but have considerably lower MS. Paramagnetic minerals have a low positive magnetic susceptibility, but cannot store properties of magnetic fields. Clay minerals are the most common paramagnetic minerals. Diamagnetic minerals have a low negative magnetic susceptibility, examples are quartz and feldspar.

When organic material is buried with sediments, often ferromagnetic components are removed by dissolution through $H_2S$ in the pore waters during burial. In such anoxic conditions, iron oxides can be reduced to iron sulphides, erasing an original signal during (early) diagenesis. When this happens, the remaining MS signal is dominated by (paramagnetic) clay minerals. In such cases, logging data are often spiky due to generally low MS, but some spikes where iron sulphide or iron carbonate nodules are part of a MS reading.

Consequently the MS signal often varies inversely with contents of authigenous bioproduction such as carbonate, silica or organic matter. MS (and other magnetic properties as e.g. the isothermal remanent magnetization) often traces terrigenous input vs. authigenic bioproduction, and MS is a frequently applied and valuable proxy (e.g., Da Silva et al., 2015 and references therein; Table 1). In marine environments, MS generally traces the influx of terrestrial material, and high MS relates to high fluvial or dust influx. Also in lacustrine environments, MS is often a tracer for the relative proportions of authigenic production (of carbonate, organic carbon and silica) and the influx of ferrigenous materials. Both GR and MS values are often related to changing amounts of detrital input into systems. This clastic input may be of aeolian or fluvial origin, the separation of such components (if more than one is relevant) may be done in the laboratory through more complex mineral magnetic analyses, but is not possible from logging (MS, GR) data.

MS measurements are commonly affected by temperature effects, and the measured MS is dependent on the temperature of the electronics (“Magnetic Susceptibility Sonde (MSS-B),” 2021) which can be corrected for. MS is a valuable method for assessing stratigraphic alternations because the measurement is non-destructive, quick, inexpensive, and repeatable. Additionally, different lithologies often have different MS signatures (e.g., Expedition 340T Scientists, 2012).

For the above mentioned reasons, MS is generally useful for correlation (e.g., Marković et al., 2015; Necula et al., 2015; Zeeden et al., 2018b), and also cyclostratigraphic studies from downhole logging or also core- and exposure data (e.g., Da Silva et al., 2013; Ulfers et al., 2021; Zeeden et al., 2016). Laboratory measurements of the MS can normalize MS over mass, which is generally less noisy than volumetric data from logging and field probes, because different pore volumes can be accounted for.

MS measurements can have a high vertical logging resolution of one to several cm, because some decentralized tools push a reading device against the borehole wall and measure the local MS. MS measurements in a borehole investigate a specific volume, and in fine grained sediments such measurements are very useful. In contrast, in coarse sediments as gravels, MS can be dominated by individual clasts with high MS, generally leading to noisy signals which are very difficult to interpret. Further, different pore volumes will influence the volumetric MS readings – which is especially important in coarse clastic materials and karstified rocks with dissolution effects.

An example of MS from downhole measurements reflecting paleo-environmental conditions is the tropical Lake Towuti on the island of Sulawesi, Indonesia (Fig. 3; Russell et al., 2016; Ulfers et al., 2021). During the last about one million years, the lake experienced repeated lake level shifts and associated changes in the oxygenation state of its bottom water. The result is an alternation of sideritic clay with increased MS deposited during cooler/drier climate, and organic rich clay with low MS from warm/wet periods. The underlying processes are likely driven by both orbital-scale changes related to eccentricity and continental ice volume (Russell et al., 2020; Ulfers et al., 2021). In this case, a suite of event layers was omitted from the dataset before applying cyclostratigraphy (Fig. 3).

### 2.3.3. Borehole Images

Although acoustic and electric image logging has been establishing for several decades, the resulting high-resolution datasets with resolution in (sub)cm spacing have not been widely used for assessing quasi-cyclic components, although valuable applications exist (see Table 1; e.g., Huang et al., 2010; Paulissen and Luthi, 2011; Reuning et al., 2006). In our opinion there remains untapped potential for investigations of the high-frequency components and their meaning and origins.

Borehole image probes provide a continuous oriented image with high resolution of the borehole walls. Figure 6 provides an illustration. Images can be gained from acoustic, electrical and optical tools (e.g., Pierdominici and Kück, 2021; Rider and Kennedy, 2011), and the originally truly circular images are usually unwrapped to a 2-D image. An acoustic image probe generates an image of the borehole wall by transmitting ultrasonic pulses from a fixed transducer with rotating mirror and records the amplitude and travel time of the signals reflected at the interface between borehole fluid and the formation (borehole wall) (Zemanek et al., 1969). The acoustic two-way travel time (TT) provides information on borehole shape (acoustic caliper), and acoustic amplitude (AMPL) is related to the acoustic reflectivity of the borehole wall which depends on the roughness and shape of the borehole wall and its acoustic properties. These AMPL and TT images are commonly displayed in color code reflecting their value range. In the AMPL image bright colors (high) indicate a strong signal (good reflection, strong contrast) and dark colors (low) are for weak to missing signals (scattered or absorbed). In the TT images, bright colours refer to short time period (fast) for the impulse to go from the transducer and back to the receiver, while dark colours indicate long time period (slow) due to the widened size of the hole. TT and AMPL signals are visualized as 360° images of the borehole wall and provide full coverage of the borehole wall, oriented using built-in triaxial accelerometers and magnetometers. A harder borehole surface translates to higher amplitude recorded by the tool, whereas softer surfaces, fractures, and void spaces are recorded at a lower relative amplitude.

The electric imager (i.e. Formation MicroImager, FMI; Formation MicroScanner, FMS) provides real-time microresistivity formation images and dip data in water-based mud (conductive borehole fluid). This probe has pads and flaps contain an array of button electrodes at constant potential and they are directly in contact with the borehole wall. Each pad injects current into the rock/sediment formation, the current flow is received at a return electrode located in the upper part of the tool. The tool, therefore, has a high-resolution capability in measuring variations from button to button (between electrodes). The resistivity of the interval between the button-electrode array and the return electrode gives rise to a low-resolution capability in the form of a background signal. This sonde yields a continuous, high-resolution electrical image of a borehole and the values are color-coded such that highly resistive material appears in bright colours and conductive material is set to dark colours. The sonde is magnetically and gravitationally oriented, allowing orientation of data. FMI and FMS imager data are the most commonly used image tool for cyclostratigraphy (Table 1).

The optical borehole imager (OBI) tool generates a continuous true high- resolution colour image of the borehole wall using a downhole camera. This tool operates only in transparent fluid in liquid-filled holes (fresh clear liquid). This requirement has limited the application of downhole cameras. A built-in high precision orientation package incorporating a 3-axis magnetometer and 3-axis accelerometer allows orientation of the images to a global reference and determination of the borehole's azimuth and inclination.

The borehole image log provides a map of the borehole walls based on specific properties which are translated to colour code for interpretation. Colour maps related to electrical, acoustic or optical contrasts reflect properties and attributes of the rock/sediment. Their analysis help to reconstruct depositional and/or tectonic history of the formation. Due to the different nature of the targeted physical properties, features visible in one of the three imager types are not necessarily visible in the others because of their different physical properties.

The image data records have a strong potential to be exploited in combination with other downhole logging measurements, such as GR, SGR and MS, for cyclostratigraphic investigations and sedimentation rate estimates. An increasing number of studies (e.g., Baumgarten et al., 2015; Hunze et al., 2013; Huret et al., 2011; Ulfers et al., 2022b; Williams et al., 2002) use spectral analysis methods applied to borehole log data to assess the frequency content of geological time-series, assisting in detailed quantitative cyclicity analysis (e.g., Li et al., 2018; Meyers, 2015; Zeeden et al., 2015). For borehole images, this type of borehole measurements are commonly analysed for structural studies such as natural and induced fractures, breakouts, structural dips but they can become also a valuable tool in sedimentary environment for identification of beddings, laminations, cross-beddings, grading, lithological boundaries, stylolites, turbidites or slumps deposits, conglomerate, viscicles, vugs and volcanic facies (e.g., Jerram et al., 2019; Pierdominici et al., 2020; Rider and Kennedy, 2011; Trice, 1999). The identification of the aforementioned features on image logs are often combined with visual inspection of drill cores (e.g., Donselaar and Schmidt, 2010; Jerram et al., 2019) to corroborate and refine the analysis and interpretation (Fig. 6).

The great advantage of the borehole images is the much higher vertical resolution (4 mm to 10 mm) than the resolution of GR and SGR (about 200 mm), allowing to discretize even extremely thin beds/layers covering a short time periods making this type of measurement potentially eligible for cyclostratigraphic analysis also for high-frequency signals such as sub-Milankovitch signals including half-precession signals (e.g., Ulfers et al., 2022a). Generally, sandstone layers show yellow-light colours, whereas siltstones and mudstones show dark-yellow and dark colour respectively in resistive borehole images. Furthermore, variation in lithology, such as from clay to carbon-rich clay, can be detected by FMS based on different resistivity values: low resistivity is registered to clay intervals whereas higher resistivity correlates with organic carbon-rich clay (Huang et al., 2010; Rider and Kennedy, 2011). Counting and marking the different layers along the stratigraphic sequence intersected by the borehole should facilitate distinguishing cycles and assigning each of them an average duration in order to estimate the age of the sediments using cyclostratigraphic methods (see section 2.6.).

The distinction of individual layers on borehole images in combination with in particular GR and MS log, usually used for cyclostratigraphic analyses, is expected to recognize cycle-stacking patterns (e.g., Muniz and Bosence, 2015; Rider and Kennedy, 2011; Ruffell and Worden, 2000). Image logs can provide detailed information on paleoclimatic changes and can represent another effective method for cyclostratigraphic analyses based on both image-logging derived proxy data and recognized cycle-stacking patterns through the use of ultra-high-resolution images. Yet, this potential is hardly tapped, and few publications use image logs for cyclostratigraphy (e.g., Williams and Pirmez, 1999).

# 3. Downhole logging data analysis

## 3.1. Suitability of proxy data and sampling rates

A key criterion in the choice of a measured proxy parameter for cyclostratigraphic investigations is a close correlation with sedimentology, and an understanding how climate and/or paleoenvironments are reflected in the proxy of choice. Further, the ability to measure a parameter with adequately fine resolution in a useful time- and cost framework is important when acquiring data for time series analysis. This requires measurements at a point, and not average values that cover a long depth/core interval. In marine and lacustrine systems, both the MS and especially the SGR (see section 3.3.) have proven to be powerful well logging proxies which often record environmentally-driven changes in sedimentation. Both proxies may provide information on the authigenic production in a system vs. influx of sediment, and SGR can provide a differentiated picture through its (K, U, Th) components and their relationships (Fig. 5).

The depth-resolution of logging data is often reduced compared to high-resolution core analysis, although deconvolution (inversion based on knowledge of the logging tool pick-up depth) may ameliorate this effect (Huret et al., 2011). It needs to be mentioned that many borehole probes integrate over a considerable depth interval and although measurements may be taken at high resolution, these may not be fully independent. Yet, given not too slow sedimentation rates, borehole logging data is proving a suitable target for cyclostratigraphic investigations. Imaging (section 3.3.3) can provide mm-scale datasets over km of boreholes.

Sedimentation rate may be slow, sometimes increasing the need for measurements at the highest possible resolution to allow for detection of sedimentary patterns and cycles, especially those cycles with shorter durations (e.g., Huret et al., 2011; Worthington, 1990). For example, at a sedimentation rate of 10 cm/kyr, and a typical sample interval of 10 cm one obtains a data point every kyr on average. This allows reconstructing cyclicity with a maximum resolution of 20 cm wavelength or 2 kyr period according to the Nyquist-Shannon sampling theorem. However, this assumes perfectly equally spaced sampling in depth and time, no gaps and zero changes in sedimentation rate, which is not the case in real geosystems. Therefore, the highest resolution cyclicity will in reality have longer wavelengths (Martinez et al., 2016).

Generally, borehole logs are considered suitable targets for astrochronology and also direct orbital tuning (e.g., Baumgarten et al., 2015; Ochoa et al., 2015; Sierro et al., 2000; Ulfers et al., 2022b), especially because of the continuous measurements (Ochoa et al., 2018).

### 3.2. Data preparation

Logging data may require depth-adjustment to a single common depth scale if the data were gathered in different logging runs (Figs. 2 and 3; Morgans-Bell et al., 2001; Weedon et al., 1999). This may be facilitated by one (usually GR) probe being connected to all runs. If logging was done in several depth intervals separately, which is usually done with considerable overlap to facilitate robust splicing, establishing a composite record in a next step is necessary. For logging datasets usually only few logging run datasets need to be tied together, in contrast to core data, where splicing is a major task and will need to assess every core and may lead to different splices based on available data (e.g., Drury et al., 2018; Wilkens et al., 2017; Zeeden et al., 2013). However, only some literature report on the borehole condition (e.g., Bahk et al., 2016; Radke et al., 2022; Rampino et al., 2000).

For time series analysis, data are commonly prepared to avoid unwanted artefacts. Logging data may require detrending, especially in unconsolidated sediments where recent sedimentation is ongoing. In such circumstances, the sediment surface and upper part commonly show e.g. low GR intensity (or MS) values due to high porosity, high water content and therefore rather low content of detrital material carrying a GR (and MS) signal (see data e.g. by Bahk et al., 2016; Baumgarten et al., 2015; Ulfers et al., 2021). Therefore, in unconsolidated sediments, detrending can be considered useful for many (if not all) applications of cyclostratigraphy. Further effects may induce trends in datasets because the interaction of drilling fluids with the borehole wall can be expected to increase with time of exposure to fluids (Ulfers et al., 2021). In contrast to many other data acquisition techniques, borehole logging data are almost always equally spaced in depth, and do not require re-sampling before analysis, or applying specific methods tailored to non-equally spaced datasets (see Trauth et al., 2007 and references therein).

Logging and core depths may differ to some extent (e.g., Giaccio et al., 2019; Morgans-Bell et al., 2001; Weedon et al., 1999), and such differences commonly increase with depth. Here, logging depth is commonly referred to as a better representation of true depth, because no issues of incomplete core recovery or sediment expansion through decompaction are expected.

Corrections for borehole diameter are useful to omit effects caused by varying diameters (Lehmann, 2010 and references therein). As for core- and sample data, outliers and possibly specific layers are useful to exclude from further analyses: tephra and turbidites are usually regarded as not useful to include in datasets for cyclostratigraphic investigations (Ulfers et al., 2021) due to their fast deposition independent of the climate regime. The effect of removing event layers is exemplified in Fig. 3.

### 3.3. Time series analysis and cyclostratigraphy applied to downhole logging data

A suite of numerical methods is available to assess quasi-cyclic data in sedimentology and Earth sciences. Among others, Trauth et al. (2007) and Weedon (2003) provide helpful overviews of signal processing and time series analysis for geoscientific purposes and specifically cyclostratigraphy. Time series analysis initially assesses the presence of (different) cyclic components in datasets, and some methods analyse their distribution over depth or time and differentiate between intervals with and without specific cyclic components.

Cyclostratigraphy ties cyclic variability in sediments and derived (borehole logging) proxy data to well established changes in insolation (Laskar et al., 2004). This is used to derive a relative time scale (e.g., Hilgen et al., 2015; Hinnov, 2000; Meyers, 2019, and references therein). Many cyclostratigraphic methods have been applied to borehole logging data, generally with the purpose of establishing relative time scales and assessing sedimentation rates. In certain geologic settings, independent age control points are available in the record. Relative ages attached to these points can result in a robust age-depth model for the entire sequence.

Spectral analysis is a widely applied and powerful tool that analyses the mean cyclicity over a whole record (Fig. 4a). It provides the intensity of specific frequencies/periods within a record. Several strong peaks generally indicate a clear climate imprint and a rather constant sedimentation rate because changes in sedimentation rate will smear out cyclic signals in the depth/time domain. Power spectra provide an invaluable method for detecting the regular cycles that forms the basis of astrochronology. However there are several critical issues associated with the correct identification of the spectral peaks as indicative of regular cyclicity rather than noise, as discussed in recent papers (e.g., Meyers, 2019; Weedon, 2022).

These cyclic components, together with their frequency relationships, allow for testing whether a dataset (and its relevant frequencies) can be matched to an (orbital) target signal (Martinson et al., 1982). Formalization of this approach was achieved by (Meyers and Sageman, 2007), who calculate an 'astronomical spectral misfit' between significant frequencies in a power spectrum from geological data and an astronomical reference for a suite of sedimentation rates. This includes associated confidence in an orbital origin of significant frequencies of a spectrum.

Assessing specific frequency ranges is very useful to extract the intensity of such signals, including amplitude relationships of e.g. precession and its eccentricity amplitude or short (~100 kyr) eccentricity and its longer term eccentricity amplitudes (Meyers, 2015, 2019; Shackleton et al., 1995; Zeeden et al., 2015). Assessment of individual frequency components can be performed through applying filters to datasets (e.g., Melnyk et al., 1994; Weedon, 2003; Zeeden et al., 2018c). Filtering results are especially informative when comparing filters of specific frequency ranges to the underlying dataset.

In cyclostratigraphy, (evolutive) power/amplitude spectra or spectrograms (Fig. 4b; see e.g., Locklair and Sageman, 2008; Molinie and Ogg, 1990; Read et al., 2020; Ulfers et al., 2021; Wonik, 2001; Worthington, 1990) and wavelet analysis (e.g., Chen et al., 2019; Prokoph and Agterberg, 1999; Wu et al., 2014) are commonly used to assess the depth/time evolution of cyclicity in a dataset. Plotting either an evolutive power spectrum or a wavelet analysis is standard in cyclostratigraphy, and visualizes the cyclic components of a dataset efficiently. For some logging datasets, which are particularly long (several km), such approaches are especially important, because orbital signals have sometimes changing characteristics. As an example, during the Mid Pleistocene Transition many geoarchives show a clear shift from ~40 kyr obliquity cycles to ~100 kyr eccentricity cycles. This can nicely be visualized using evolutive approaches (e.g. Fig. 4).

An evolutive (sliding window) correlation between data- and orbital template spectra to search for the most suitable sedimentation rate(s) was established by (Martinson et al., 1982). It was formalized by (Li et al., 2018), and its value for constructing time scales was highlighted. It is now increasingly used in cyclostratigraphy, and also on logging data (e.g., Du et al., 2020; Gong, 2021; Li et al., 2019a; Read et al., 2020; Zhang et al., 2020).

Several methods use the precession or eccentricity amplitude patterns in combination with power spectral properties to investigate the presence of insolation-driven sedimentary cycles, and test a multitude of different sedimentation rates for a useful fit between precession amplitude and eccentricity or short eccentricity and its amplitude patterns (Meyers, 2019, 2015). The timeOpt and timeOptTemplate methods as implemented in R (Meyers, 2019, 2015, 2014; R Core Team, 2022) are especially useful in tying logging data to time (Figs. 2e and 7). This is because the amplitude patterns are more diagnostic for an orbital imprint than frequency patterns (Hilgen et al., 2015; Shackleton et al., 1995; Zeeden et al., 2019, 2015). The possibility to test a suite of sedimentation rates (timeOpt) and at the same time also trends in sedimentation rate (timeOptTemplate) allows the assessment of best fits of precession or eccentricity amplitudes and their modulating eccentricity/long eccentricity components.

The timeOptTemplate method has been successfully applied to downhole GR data from e.g., Lake Ohrid to estimate average sedimentation rates (Ulfers et al., 2022b). In this publication, the sedimentation model is compared to an independently developed sedimentation rate model that is based on the correlation of borehole-GR data to the LR04 benthic stack from (Lisiecki and Raymo, 2005a) and a linear trend of these. Both models include the same initial data, but use different methods that result in very similar sedimentation rates (Fig. 7). For methods such as TimeOptTemplate, the quality of recorded orbital cycles in the output data is apparently of crucial relevance; already (Shackleton et al., 1995) clearly indicating its dependency on data quality and associated limitations (cf. Ulfers et al., 2022b). The limitations of the method are evident at drill sites in Lake Ohrid which contain only a weak precession signal (Ulfers et al., 2022b).

### 3.4. Multivariate methods for paleoclimatic investigations

To construct continuous lithological profiles, cluster analysis based on borehole logging data is a most powerful tool. Detrending logging data may be applied before cluster analysis to counter trends in the dataset that are related to compaction or fluid intrusion into the sediments of the upper borehole. Clearly, the more logging data available, and the more aspects of lithology these logging data encompass, the more differentiated the result of such a cluster analysis can be (Figs. 2d, 8). Thereby, cluster analysis may base on logging data only (e.g., Bücker et al., 2000; Fresia et al., 2017; Hunze and Wonik, 2009, 2007), or a combination of logging- and core- data (e.g., Baumgarten et al., 2014). Such a quantitative approach of establishing a stratigraphic description is less commonly applied based on core- or exposure data, although such studies exist (e.g., Szabó et al., 2019). This is probably due to the fact that for cores and exposures, semi-quantitative descriptions and visual impression along with experience are often considered more valuable although less reproducible.

Although logging data include information about the physical properties of sediments, they cannot always directly be related to lithology; however, appropriate measurements can provide clear evidence of lithology. While logging data can provide clues to lithology, the ideal evidence of lithology is a visible rock or core that can be assessed by eye and analysed using methods tailored to specific questions. Generally, the more logging information available and the better the geology of a region is understood, the more robust the interpretation of the sediment/rock type based on logging data. When specific sediment/rock types are expected and the geological background is known, one or few logging parameters may characterize a dataset, and allow for correlation between logs and exposures (e.g., Broding et al., 1952; Prokoph and Agterberg, 1999; Read et al., 2020).

The quality of results of a cluster analysis improves with increasing contrast in the physical properties of the (sedimentary) rocks. In Lake Ohrid, for example, there are primarily two types of sediment which clearly differ from each other in their physical properties (Fig. 8). Besides several other parameters, GR is an important proxy in this context. The results of the cluster analysis demonstrate a high level of similarity compared to the core description (Fig. 8). Cluster analysis can be applied to other sites in the

Ohrid Basin, and provides additional information about parts in the sediment succession where core loss occurred (Ulfers et al., 2022b).

### 3.5. Example of integrating exposure, core- and downhole logging with cyclostratigraphy

The Rapid Global Geological Events (RGGE) project (Gallois, 2000) is taken as example of downhole logging, time series analysis and cyclostratigraphy here. The project involved logging of the type locality of the Kimmeridge Clay in Dorset/UK, including exposure MS measurements and portable GR logging in the field (Morgans-Bell et al., 2001). Two boreholes were drilled near the exposure cliffs, and a full suite of downhole logs were generated (Gallois, 2000; his Table 1) in addition to continuous coring of this mudrock formation. Weedon et al., (1999) could show that the MS time series from the exposure, core and downhole could be correlated in detail (Weedon et al., 1999; their Fig. 9). Weedon et al (2004) then used the core MS on the common depth scale, combined with downhole Photoelectric Factor and Total GR logs from the boreholes, to demonstrate regular cyclicity linked to Milankovitch cycles. A dominant frequency was assigned to obliquity, also because of a secondary cyclic component with about half its wavelength (Weedon et al., 2004). Based on this realization, Weedon et al. (2004) then provided the first estimate of the duration of the Kimmeridgian Stage from cycle counting to be 3.6 Ma for the Early Kimmeridgian, and 3.9 Ma for the Late Kimmeridgian. They also provide durations for a suite of Ammonite zones. Later, Huang et al (2010) used FMS micrologging from the RGGE downhole logging to re-examine the cyclicity, and essentially confirmed the astrochronology of Weedon et al (2004). They, however, used mainly the longer 405 kyr cycle, and suggested an almost identical duration of the Lower Kimmeridgian, and a somewhat shorter duration (3.32 Ma) for the Upper Kimmeridgian – a close fit given the Jurassic time ~150 Ma ago.

## 4. <u>Summary</u>

Here we review properties of borehole logging data and time series analysis which are relevant for geoscientists with a broad range of expertise. Especially, we point out some relevant differences to core data. Logging data can encompass 10s to 1000s of meters of equally-spaced data in high resolution, a most desirable goal for many scientists working on geological time series analysis. An increasing suite of studies shows the value of borehole logging data in the context of sedimentology, stratigraphy and paleoclimatology. Especially for Quaternary and not fully consolidated sediments, detrending is useful and can ease relating depth-derived properties to astronomical properties. However, datasets often represent composites, especially when derived from unconsolidated sediments. Multivariate logging datasets generally cannot be perfectly synchronized, but deviations from synchrony can be expected to be small. Several downhole logging data proxies are often related to lithology and paleoclimate, and are therefore valuable targets for astrochronology; these include SGR and MS. Further, we suggest that the value of image data is not yet fully tapped for time series analyses, and we will test these data in future for their value of revealing quasi-cyclic sediment alterations. We highlight that borehole logging data have the potential to contribute more to the fields of sedimentology and Earth science in general. This is supported by the increasing number of studies using imaging logs to assess short term sediment- and climate variability.

## 5. Acknowledgements

The authors thank the LIAG for its constructive environment and support of logging facilities. This research was funded by the Deutsche Forschungsgemeinschaft (DFG, German Research Foundation), - grant numbers WO672/5, WO672/9, WO672/10, WO672/15, WO672/18, ZE 1145/10. We thank Graham Weedon for constructive and detailed reviews, which clearly helped improve this manuscript.

## References

Aboubacar, M.S.I., Heng, Z., Li, J., Ousmane, B.I., Cai, Z., 2022. Prediction of petrophysical classes and reservoir beds through microfacies and pore types characterization, Tahe Ordovician naturally fractured vuggy carbonates. Interpretation 10, T837–T854. https://doi.org/10.1190/INT-2022-0008.1

Bahk, J.-J., Um, I.-K., Yi, B.-Y., Yoo, D.-G., 2016. Paleoceanographic implications and cyclostratigraphy of variations in well-log data from the western slope of the Ulleung Basin, East Sea. Quat. Int., Paleoenvironmental studies in the Korean Peninsula and adjacent geographic areas IV 392, 58–68. https://doi.org/10.1016/j.quaint.2015.08.023

Barthès, V., Pozzi, J.P., Vibert-Charbonnel, P., Thibal, J., Mélières, M.A., 1999. High-resolution chronostratigraphy from downhole susceptibility logging tuned by palaeoclimatic orbital frequencies. Earth Planet. Sci. Lett. 165, 97–116. https://doi.org/10.1016/S0012-821X(98)00214-3

Baumgarten, H., Wonik, T., 2015. Cyclostratigraphic studies of sediments from Lake Van (Turkey) based on their uranium contents obtained from downhole logging and paleoclimatic implications. Int. J. Earth Sci. 104, 1639–1654. https://doi.org/10.1007/s00531-014-1082-x

Baumgarten, H., Wonik, T., Kwiecien, O., 2014. Facies characterization based on physical properties from downhole logging for the sediment record of Lake Van, Turkey. Quat. Sci. Rev. 104, 85–96. https://doi.org/10.1016/j.quascirev.2014.03.016

Baumgarten, H., Wonik, T., Tanner, D.C., Francke, A., Wagner, B., Zanchetta, G., Sulpizio, R., Giaccio, B., Nomade, S., 2015. Age–depth model of the past 630 kyr for Lake Ohrid (FYROM/Albania) based on cyclostratigraphic analysis of downhole gamma ray data. Biogeosciences 12, 7453–7465. https://doi.org/10.5194/bg-12-7453-2015

Beil, S., Kuhnt, W., Holbourn, A., Scholz, F., Oxmann, J., Wallmann, K., Lorenzen, J., Aquit, M., Chellai, E.H., 2020. Cretaceous oceanic anoxic events prolonged by phosphorus cycle feedbacks. Clim. Past 16, 757–782. https://doi.org/10.5194/cp-16-757-2020

Beil, S., Kuhnt, W., Holbourn, A.E., Aquit, M., Flögel, S., Chellai, E.H., Jabour, H., 2018. New insights into Cenomanian paleoceanography and climate evolution from the Tarfaya Basin, southern Morocco. Cretac. Res. 84, 451–473. https://doi.org/10.1016/j.cretres.2017.11.006

Boulila, S., Brange, C., Cruz, A.M., Laskar, J., Gorini, C., Reis, T.D., Silva, C.G., 2020. Astronomical pacing of Late Cretaceous third- and second-order sea-level sequences in the Foz do Amazonas Basin. Mar. Pet. Geol. 117, 104382. https://doi.org/10.1016/j.marpetgeo.2020.104382

Boulila, S., Dupont-Nivet, G., Galbrun, B., Bauer, H., Châteauneuf, J.-J., 2021. Age and driving mechanisms of the Eocene–Oligocene transition from astronomical tuning of a lacustrine record (Rennes Basin, France). Clim. Past 17, 2343–2360. https://doi.org/10.5194/cp-17-2343-2021

Broding, R.A., Zimmerman, C.W., Somers, E.V., Wilhelm, E.S., Stripling, A.A., 1952. Magnetic Well Logging. Geophysics 17, 1–26. https://doi.org/10.1190/1.1437736

Brown, E.T., Caballero, M., Cabral Cano, E., Fawcett, P.J., Lozano-García, S., Ortega, B., Pérez, L., Schwalb, A., Smith, V., Steinman, B.A., Stockhecke, M., Valero-Garcés, B., Watt, S., Wattrus, N.J., Werne, J.P., Wonik, T., Myrbo, A.E., Noren, A.J., O'Grady, R., Schnurrenberger, D., the MexiDrill Team, 2019. Scientific drilling of Lake Chalco, Basin of Mexico (MexiDrill). Sci Dril 26, 1–15. https://doi.org/10.5194/sd-26-1-2019

Bücker, C., Jarrard, R.D., Wonik, T., Brink, J., 2000. Analysis of downhole logging data from CRP-2/2A, Victoria Land Basin, Antarctica: a multivariate statistical approach. Terra Antartica 7, 299–310.

Cao, H., Jin, S., Sun, M., Wang, H., 2016. Astronomical forcing of sedimentary cycles of Late Eocene Liushagang Formation in the Bailian Sag, Fushan Depression, Beibuwan Basin, South China Sea. J. Cent. South Univ. 23, 1427–1438. https://doi.org/10.1007/s11771-016-3195-9

Cheddadi, R., Rossignol-Strick, M., 1995. Eastern Mediterranean Quaternary paleoclimates from pollen and isotope records of marine cores in the Nile Cone Area. Paleoceanography 10, 291–300. https://doi.org/10.1029/94PA02672

Chen, G., Gang, W., Liu, Y., Wang, N., Guo, Y., Zhu, C., Cao, Q., 2019. High-resolution sediment accumulation rate determined by cyclostratigraphy and its impact on the organic matter abundance of the hydrocarbon source rock in the Yanchang Formation, Ordos Basin, China. Mar. Pet. Geol. 103, 1–11. https://doi.org/10.1016/j.marpetgeo.2019.01.044

Chen, Z., Li, F., Zhang, P., 2022. High-resolution terrestrial record of orbital climate forcing in the coal-bearing Middle Jurassic Yan'an Formation, Ordos Basin, North China. Geol. J. 57, 1873–1890. https://doi.org/10.1002/gj.4385

Cheng, L., Wang, J., Wan, Y., Fu, X., Zhong, L., 2017. Astrochronology of the Middle Jurassic Buqu Formation (Tibet, China) and its implications for the Bathonian time scale. Palaeogeogr. Palaeoclimatol. Palaeoecol. 487, 51–58. https://doi.org/10.1016/j.palaeo.2017.08.018

Christensen, B.A., Renema, W., Henderiks, J., Vleeschouwer, D.D., Groeneveld, J., Castañeda, I.S., Reuning, L., Bogus, K., Auer, G., Ishiwa, T., McHugh, C.M., Gallagher, S.J., Fulthorpe, C.S., 2017. Indonesian Throughflow drove Australian climate from humid Pliocene to arid Pleistocene. Geophys. Res. Lett. 44, 6914–6925. https://doi.org/10.1002/2017GL072977

Colman, S.M., Peck, J.A., Karabanov, E.B., Carter, S.J., Bradbury, J.P., King, J.W., Williams, D.F., 1995. Continental climate response to orbital forcing from biogenic silica records in Lake Baikal. Nature 378, 769–771. https://doi.org/10.1038/378769a0

Cooper, P., 1995. Milankovitch cycles from Fourier analysis of logs from Sites 865 and 866: Northwest Pacific atolls and guyots. Proc. Ocean Drill. Program Sci. Results 142, 317–327. https://doi.org/10.2973/odp.proc.sr.143.236.1995

Czymzik, M., Muscheler, R., Brauer, A., Adolphi, F., Ott, F., Kienel, U., Dräger, N., S\lowiński, M., Aldahan, A., Possnert, G., 2015. Solar cycles and depositional processes in annual 10 Be from two varved lake sediment records. Earth Planet. Sci. Lett. 428, 44–51.

Da Silva, A.C., De Vleeschouwer, D., Boulvain, F., Claeys, P., Fagel, N., Humblet, M., Mabille, C., Michel, J., Sardar Abadi, M., Pas, D., Dekkers, M.J., 2013. Magnetic susceptibility as a high-resolution correlation tool and as a climatic proxy in Paleozoic rocks – Merits and pitfalls: Examples from the Devonian in Belgium. Mar. Pet. Geol. 46, 173–189. https://doi.org/10.1016/j.marpetgeo.2013.06.012

Da Silva, A.C., Whalen, M.T., Hladil, J., Chadimova, L., Chen, D., Spassov, S., Boulvain, F., Devleeschouwer, X., 2015. Magnetic susceptibility application: a window onto ancient environments and climatic variations: foreword. Geol. Soc. Lond. Spec. Publ. 414, 1–13. https://doi.org/10.1144/SP414.12

De Vleeschouwer, D., Parnell, A.C., 2014. Reducing time-scale uncertainty for the Devonian by integrating astrochronology and Bayesian statistics. Geology 42, 491–494. https://doi.org/10.1130/G35618.1

Donselaar, M.E., Schmidt, J.M., 2010. The application of borehole image logs to fluvial facies interpretation.

Drury, A.J., Westerhold, T., Hodell, D., Röhl, U., 2018. Reinforcing the North Atlantic backbone: revision and extension of the composite splice at ODP Site 982. Clim. Past 14, 321–338. https://doi.org/10.5194/cp-14-321-2018

Du, W., Ji, Y., Chen, G., Wu, H., Gao, C., Li, S., Zhang, Y., 2020. Cyclostratigraphy and astronomical tuning during the Oligocene in the Jizhong Depression, Bohai Bay Basin, northeastern China. Palaeogeogr. Palaeoclimatol. Palaeoecol. 554, 109803. https://doi.org/10.1016/j.palaeo.2020.109803

Expedition 340T Scientists, 2012. Integrated Ocean Drilling Program Expedition 340T Preliminary Report, IODP Preliminary Report. Integrated Ocean Drilling Program. https://doi.org/10.2204/iodp.pr.340T.2012

Falahatkhah, O., Ciabeghodsi, A.A., Kadkhodaie, A., 2020. Comparison of variations in sediment accumulation rates of the upper part of Zakeen Formation through cyclostratigraphic study in 2SK-1 and 2SKD-1 wells in Salman gas field. J. Stratigr. Sedimentol. Res. 36, 1–22. https://doi.org/10.22108/jssr.2020.120178.1130

Falahatkhah, O., Kadkhodaie, A., Ciabeghodsi, A.A., Li, M., 2021a. Cyclostratigraphy of the Lower Triassic Kangan Formation in the Salman gas field, eastern Persian Gulf, Iran. Palaeogeogr. Palaeoclimatol. Palaeoecol. 561, 110045. https://doi.org/10.1016/j.palaeo.2020.110045

Falahatkhah, O., Kordi, M., Fatemi, V., Koochi, H.H., 2021b. Recognition of Milankovitch cycles during the Oligocene–Early Miocene in the Zagros Basin, SW Iran: Implications for paleoclimate and sequence stratigraphy. Sediment. Geol. 421, 105957. https://doi.org/10.1016/j.sedgeo.2021.105957

Farouk, S., Abdeldaim, A., Thibault, N., Aref, M., Elfiki, W., El-Kahtany, K., 2022a. Cyclostratigraphy and eccentricity tunning of the middle Miocene succession, Gulf of Suez, Egypt: Astronomical age dating and undetected hiatus. Mar. Pet. Geol. 143, 105771. https://doi.org/10.1016/j.marpetgeo.2022.105771

Farouk, S., Ren, C., Abdeldaim, A., Salama, A., Wu, H., El-Kahtany, K., Zaky, A.S., 2022b. An astronomical time scale of early Pliocene from the Mediterranean Sea, Egypt. Glob. Planet. Change 215, 103869. https://doi.org/10.1016/j.gloplacha.2022.103869

Fischer, A.G., 1995. Cyclostratigraphy, Quo Vadis? Geol. Soc. Lond. Spec. Publ. 85, 199–204. https://doi.org/10.1144/GSL.SP.1995.085.01.12

Fischer, A.G., Herbert, T.D., Napoleone, G., Silva, I.P., Ripepe, M., 1991. Albian Pelagic Rhythms (Piobbico Core). J. Sediment. Res. 61.

Fischer, A.G., Roberts, L.T., 1991. Cyclicity in the Green River Formation (lacustrine Eocene) of Wyoming. J. Sediment. Res. 61, 1146–1154. https://doi.org/10.1306/D4267852-2B26-11D7-8648000102C1865D

Francke, Alexander, Wagner, B., Just, J., Leicher, N., Gromig, R., Baumgarten, H., Vogel, H., Lacey, J.H., Sadori, L., Wonik, T., Leng, M.J., Zanchetta, G., Sulpizio, R., Giaccio, B., 2016. Sedimentological processes and environmental variability at Lake Ohrid (Macedonia, Albania) between 637 ka and the present. Biogeosciences 13, 1179–1196. https://doi.org/10.5194/bg-13-1179-2016

Francke, A., Wagner, B., Just, J., Leicher, N., Gromig, R., Baumgarten, H., Vogel, H., Lacey, J.H., Sadori, L., Wonik, T., Leng, M.J., Zanchetta, G., Sulpizio, R., Giaccio, B., 2016. Sedimentological processes and environmental variability at Lake Ohrid (Macedonia, Albania) between 637 ka and the present. Biogeosciences 13, 1179–1196. https://doi.org/10.5194/bg-13-1179-2016

Fresia, B., Ross, P.-S., Gloaguen, E., Bourke, A., 2017. Lithological discrimination based on statistical analysis of multi-sensor drill core logging data in the Matagami VMS district, Quebec, Canada. Ore Geol. Rev. 80, 552–563. https://doi.org/10.1016/j.oregeorev.2016.07.019

Friedrich, T., Timmermann, A., Tigchelaar, M., Timm, O.E., Ganopolski, A., 2016. Nonlinear climate sensitivity and its implications for future greenhouse warming. Sci. Adv. 2, e1501923. https://doi.org/10.1126/sciadv.1501923

Fritzen, M.R., Cagliari, J., Candido, M., Lavina, E.L.C., 2019. Tidal bar cyclicity record in the Lower Permian: The Rio Bonito Formation, Paraná Basin, southern Brazil. Sediment. Geol. 381, 76–83. https://doi.org/10.1016/j.sedgeo.2018.12.011

Gallois, R., 2000. The stratigraphy of the Kimmeridge Clay Formation (Upper Jurassic) in the RGGE Project boreholes at Swanworth Quarry and Metherhills, south Dorset. Proc. Geol. Assoc. 111, 265–280. https://doi.org/10.1016/S0016-7878(00)80019-X

Gao, Y., Fu, X., Li, Y., Wan, Y., Wang, Z., Song, C., Shen, H., Lin, F., 2020. Demise of the Middle Jurassic carbonate platform: Responses to sea-level fall in the Qiangtang Basin, Eastern Tethys. Geol. J. 55, 7935–7952. https://doi.org/10.1002/gj.3923

Giaccio, B., Leicher, N., Mannella, G., Monaco, L., Regattieri, E., Wagner, B., Zanchetta, G., Gaeta, M., Marra, F., Nomade, S., Palladino, D.M., Pereira, A., Scheidt, S., Sottili, G., Wonik, T., Wulf, S., Zeeden, C., Ariztegui, D., Cavinato, G.P., Dean, J.R., Florindo, F., Leng, M.J., Macrì, P., Niespolo, E., Renne, P.R., Rolf, C., Sadori, L., Thomas, C., Tzedakis, P.C., 2019. Extending the tephra and palaeoenvironmental record of the Central Mediterranean back to 430 ka: A new core from Fucino Basin, central Italy. Quat. Sci. Rev. 225, 106003. https://doi.org/10.1016/j.quascirev.2019.106003

Goldberg, D., 1997. The role of downhole measurements in marine geology and geophysics. Rev. Geophys. 35, 315–342. https://doi.org/10.1029/97RG00221

Goldhammer, R., Oswald, E., Dunn, P.A., 1994. High-frequency, glacio-eustatic cyclicity in the Middle Pennsylvanian of the Paradox Basin: an evaluation of Milankovitch forcing. Orbital Forcing Cycl. Seq. 19, 243–283.

Golovchenko, X., O'Connell, S.B., Jarrard, R., 1990. Sediemntary response to paleoclimate from downhole logs at Site 639, Antarctic Contoinental margin. Proc. Ocean Drill. Program Sci. Results 113, 239–251. https://doi.org/10.2973/odp.proc.sr.113.191.1990

Gong, Z., 2021. Cyclostratigraphy of the Cryogenian Fiq Formation, Oman and its implications for the age of the Marinoan glaciation. Glob. Planet. Change 204, 103584. https://doi.org/10.1016/j.gloplacha.2021.103584

Gong, Z., Li, M., 2020. Astrochronology of the Ediacaran Shuram carbon isotope excursion, Oman. Earth Planet. Sci. Lett. 547, 116462. https://doi.org/10.1016/j.epsl.2020.116462

Guo, D., Jin, Z., 2021. Astronomical time scale of a Middle Eocene lacustrine sequence from the Dongpu Sag, Bohai Bay Basin, Eastern China. J. Asian Earth Sci. 214, 104747. https://doi.org/10.1016/j.jseaes.2021.104747

Hagelberg, T.K., Pisias, N., 1990. Nonlinear response of Pliocene climate to orbital forcing: Evidence from the eastern equatorial Pacific. Paleoceanography 5, 595–617.

Hernández-Molina, F.J., Sierro, F.J., Llave, E., Roque, C., Stow, D.A.V., Williams, T., Lofi, J., Schee, M.V. der, Arnáiz, A., Ledesma, S., Rosales, C., Rodríguez-Tovar, F.J., Pardo-Igúzquiza, E., Brackenridge, R.E., 2016. Evolution of the gulf of Cadiz margin and southwest Portugal contourite depositional system: Tectonic, sedimentary and paleoceanographic implications from IODP expedition 339. Mar. Geol. 377, 7–39. https://doi.org/10.1016/j.margeo.2015.09.013

Hilgen, F.J., Hinnov, L.A., Aziz, H.A., Abels, H.A., Batenburg, S., Bosmans, J.H.C., Boer, B. de, Hüsing, S.K., Kuiper, K.F., Lourens, L.J., Rivera, T., Tuenter, E., Wal, R.S.W.V. de, Wotzlaw, J.-F., Zeeden, C., 2015. Stratigraphic continuity and fragmentary sedimentation: the success of cyclostratigraphy as part of integrated stratigraphy. Geol. Soc. Lond. Spec. Publ. 404, 157–197. https://doi.org/10.1144/SP404.12

Hinnov, L.A., 2000. New Perspectives on Orbitally Forced Stratigraphy. Annu. Rev. Earth Planet. Sci. 28, 419–475. https://doi.org/10.1146/annurev.earth.28.1.419

Hinnov, L.A., Hilgen, F.J., 2012. Chapter 4 - Cyclostratigraphy and Astrochronology, in: Gradstein, F.M., Ogg, J.G., Schmitz, M.D., Ogg, G.M. (Eds.), The Geologic Time Scale. Elsevier, Boston, pp. 63–83.

Hodell, D.A., Channell, J.E.T., 2016. Mode transitions in Northern Hemisphere glaciation: co-evolution of millennial and orbital variability in Quaternary climate. Clim Past 12, 1805–1828. https://doi.org/10.5194/cp-12-1805-2016

Huang, C., Hesselbo, S.P., Hinnov, L., 2010. Astrochronology of the late Jurassic Kimmeridge Clay (Dorset, England) and implications for Earth system processes. Earth Planet. Sci. Lett. 289, 242–255. https://doi.org/10.1016/j.epsl.2009.11.013

Huang, C., Hinnov, L., 2019. Astronomically forced climate evolution in a saline lake record of the middle Eocene to Oligocene, Jianghan Basin, China. Earth Planet. Sci. Lett. 528, 115846. https://doi.org/10.1016/j.epsl.2019.115846

Huang, H., Gao, Y., Jones, M.M., Tao, H., Carroll, A.R., Ibarra, D.E., Wu, H., Wang, C., 2020. Astronomical forcing of Middle Permian terrestrial climate recorded in a large paleolake in northwestern China. Palaeogeogr. Palaeoclimatol. Palaeoecol. 550, 109735. https://doi.org/10.1016/j.palaeo.2020.109735

Huang, H., Gao, Y., Ma, C., Jones, M.M., Zeeden, C., Ibarra, D.E., Wu, H., Wang, C., 2021. Organic carbon burial is paced by a 173-ka obliquity cycle in the middle to high latitudes. Sci. Adv. 7. https://doi.org/10.1126/sciadv.abf9489

Hunze, S., Schröder, H., Kuhn, G., Wonik, T., 2013. Lithostratigraphy determined from downhole logs in the AND-2A borehole, southern Victoria Land Basin, McMurdo Sound, Antarctica. Geosphere 9, 63–73. https://doi.org/10.1130/GES00774.1

Hunze, S., Wonik, T., 2009. Sediment Input into the Heidelberg Basin as determined from Downhole Logs. EG Quat. Sci. J. 57, 367–381. https://doi.org/10.3285/eg.57.3-4.5

Hunze, S., Wonik, T., 2007. Lithological and structural characteristics of the Lake Bosumtwi impact crater, Ghana: Interpretation of acoustic televiewer images. Meteorit. Planet. Sci. 42, 779–792. https://doi.org/10.1111/j.1945-5100.2007.tb01074.x

Huret, E., Thiesson, J., Tabbagh, A., Galbrun, B., Collin, P.-Y., 2011. Improvement of cyclostratigraphic studies by processing of high-resolution magnetic susceptibility logging: Example of PEP1002 borehole (Bure, Meuse, France). Comptes Rendus Geosci. 343, 379–386. https://doi.org/10.1016/j.crte.2011.04.002

Hüsing, S.K., Kuiper, K.F., Link, W., Hilgen, F.J., Krijgsman, W., 2009. The upper Tortonian–lower Messinian at Monte dei Corvi (Northern Apennines, Italy): Completing a Mediterranean reference section for the Tortonian Stage. Earth Planet. Sci. Lett. 282, 140–157. https://doi.org/10.1016/j.epsl.2009.03.010

Jarrard, R.D., Arthur, M.A., 1989. Milankovitch paleoceanographic cycles in geophysical logs from ODP Leg 105, Labrador Sea and Baffin Bay.

Jerram, D.A., Millett, J.M., Kück, J., Thomas, D., Planke, S., Haskins, E., Lautze, N., Pierdominici, S., 2019. Understanding volcanic facies in the subsurface: a combined core, wireline logging and image log data set from the PTA2 and KMA1 boreholes, Big Island, Hawai`i. Sci. Drill. 25, 15–33. https://doi.org/10.5194/sd-25-15-2019

Jin, S., Liu, S., Li, Z., Chen, A., Ma, C., 2022. Astrochronology of a middle Eocene lacustrine sequence and sedimentary noise modeling of lake-level changes in Dongying Depression, Bohai Bay Basin. Palaeogeogr. Palaeoclimatol. Palaeoecol. 585, 110740. https://doi.org/10.1016/j.palaeo.2021.110740

Johnsson, M.J., Reynolds, R.C., 1986. Clay mineralogy of shale-limestone rhythmites in the Scaglia rossa (Turonian-Eocene), Italian Apennines. J. Sediment. Res. 56, 501–509. https://doi.org/10.1306/212F896D-2B24-11D7-8648000102C1865D

Kaboth-Bahr, S., Koutsodendris, A., Lu, Y., Nakajima, K., Zeeden, C., Appel, E., Fang, X., Rösler, W., Friedrich, O., Pross, J., 2020. A late Pliocene to early Pleistocene (3.3-2.1 Ma) orbital chronology for the Qaidam Basin paleolake (NE Tibetan Plateau) based on the SG-1b drillcore record. Newsl. Stratigr. https://doi.org/10.1127/nos/2020/0555

Korngreen, D., Orlov-Labkovsky, O., Bialik, O.M., Benjamini, C., 2013. The Permian-Triassic transition in the central coastal plain of Israel (North Arabian Plate margin), David 1 borehole. PALAIOS 28, 491–508. https://doi.org/10.2110/palo.2012.p12-042r

Kouamelan, K.S., Zou, C., Assie, K.R., Peng, C., N'dri, K.A., Mondah, O.R., 2021. Upper Cretaceous paleoenvironmental changes and petrophysical responses in lacustrine record (Songliao Basin, NE China) and marine sedimentary deposit (Goban Spur Basin, NW Europe). J. Geophys. Eng. 18, 23–46. https://doi.org/10.1093/jge/gxaa066

Kroon, D., Williams, T., Pirmez, C., Spezzaferri, S., Sato, T., Wright, J., 2000. CoupledEarlyPliocene-Middle Miocene Bio-Cyclostratigraphy of Site 1006 reveals orbitally induced cyclicity patterns of great Bahama Bank carbonate production. Presented at the Proceedings of the Ocean Drilling Program. Scientific results, Ocean Drilling Program, pp. 155–166.

Kuhnt, W., Nederbragt, A., Leine, L., 1997. Cyclicity of Cenomanian-Turonian organic-carbon-rich sediments in the Tarfaya Atlantic Coastal Basin (Morocco). Cretac. Res. 18, 587–601. https://doi.org/10.1006/cres.1997.0076

Lai, F., Huang, Z.-H., Zhu, Z., Xu, S., Xia, W., Luo, H., 2018. Monte Carlo Clean Spectral Analysis Method For Detecting the Stratigraphic Cycles Based On High-resolution Electrical Image Log Data. J. Environ. Eng. Geophys. 22, 325–337. https://doi.org/10.2113/JEEG22.4.325

Lang, J., Zhang, T., Zhu, H., Zeng, J., Liang, X., 2018. Cyclostratigraphy under the Control of Orbital Periods: A Case Study of the Late Ordovician-early Silurian Strata. J. Coast. Res. 369–374. https://doi.org/10.2112/SI83-061.1

Laskar, J., Robutel, P., Joutel, F., Gastineau, M., Correia, A.C.M., Levrard, B., 2004. A long-term numerical solution for the insolation quantities of the Earth. Astron. Astrophys. 428, 261–285. https://doi.org/10.1051/0004-6361:20041335

Laurin, J., Čech, S., Uličný, D., Štaffen, Z., Svobodová, M., 2014. Astrochronology of the Late Turonian: implications for the behavior of the carbon cycle at the demise of peak greenhouse. Earth Planet. Sci. Lett. 394, 254–269. https://doi.org/10.1016/j.epsl.2014.03.023

Laurin, J., Uličn;ý, D., 2004. Controls on a Shallow-Water Hemipelagic Carbonate System Adjacent to a Siliciclastic Margin: Example from Late Turonian of Central Europe. J. Sediment. Res. 74, 697–717. https://doi.org/10.1306/020904740697

Lefranc, M., Beaudoin, B., Chilès, J.P., Guillemot, D., Ravenne, C., Trouiller, A., 2008. Geostatistical characterization of Callovo–Oxfordian clay variability from high-resolution log data. Phys. Chem. Earth Parts ABC 33, S2–S13. https://doi.org/10.1016/j.pce.2008.10.053

Lehmann, K., 2010. Environmental corrections to gamma-ray log data: Strategies for geophysical logging with geological and technical drilling. J. Appl. Geophys. 70, 17–26. https://doi.org/10.1016/j.jappgeo.2009.10.001

Leicher, N., Giaccio, B., Zanchetta, G., Sulpizio, R., Albert, P.G., Tomlinson, E.L., Lagos, M., Francke, A., Wagner, B., 2021. Lake Ohrid's tephrochronological dataset reveals 1.36 Ma of Mediterranean explosive volcanic activity. Sci. Data 8, 231. https://doi.org/10.1038/s41597-021-01013-7

Leu, K., Zeeden, C., Wonik, T., Mann, T., Erbacher, J., Bornemann, A., 2022. Litho-and cyclostratigraphy of the Aalenian Opalinusclay Formation in the Swabian Alb deduced from downhole logging data. Copernicus Meetings.

Li, M., Hinnov, L., Kump, L., 2019a. Acycle: Time-series analysis software for paleoclimate research and education. Comput. Geosci. 127, 12–22. https://doi.org/10.1016/j.cageo.2019.02.011

Li, M., Huang, C., Ogg, J., Zhang, Y., Hinnov, L., Wu, H., Chen, Z.-Q., Zou, Z., 2019b. Paleoclimate proxies for cyclostratigraphy: Comparative analysis using a Lower Triassic marine section in South China. Earth-Sci. Rev. 189, 125–146. https://doi.org/10.1016/j.earscirev.2019.01.011

Li, M., Kump, L.R., Hinnov, L.A., Mann, M.E., 2018. Tracking variable sedimentation rates and astronomical forcing in Phanerozoic paleoclimate proxy series with evolutionary correlation coefficients and hypothesis testing. Earth Planet. Sci. Lett. 501, 165–179. https://doi.org/10.1016/j.epsl.2018.08.041

Li, X., Huang, Y., Zhang, Z., Wang, C., 2022. Chemical weathering characteristics of the Late Cretaceous Nenjiang Formation from the Songliao Basin (Northeastern China) reveal prominent Milankovitch band variations. Palaeogeogr. Palaeoclimatol. Palaeoecol. 601, 111130. https://doi.org/10.1016/j.palaeo.2022.111130

Li, Y., Shao, L., Yan, Z., Hou, H., Tang, Y., Large, D.J., 2018. Net primary productivity and its control of the Middle Jurassic peatlands: An example from the southern Junggar coalfield. Sci. China Earth Sci. 61, 1633–1643.

Liebrand, D., Bakker, A.T.M. de, Beddow, H.M., Wilson, P.A., Bohaty, S.M., Ruessink, G., Pälike, H., Batenburg, S.J., Hilgen, F.J., Hodell, D.A., Huck, C.E., Kroon, D., Raffi, I., Saes, M.J.M., Dijk, A.E. van, Lourens, L.J., 2017. Evolution of the early Antarctic ice ages. Proc. Natl. Acad. Sci. 201615440. https://doi.org/10.1073/pnas.1615440114

Lisiecki, L.E., Raymo, M.E., 2005a. A Pliocene-Pleistocene stack of 57 globally distributed benthic δ18O records. Paleoceanography 20. https://doi.org/10.1029/2004PA001071

Lisiecki, L.E., Raymo, M.E., 2005b. A Pliocene-Pleistocene stack of 57 globally distributed benthic δ18O records. Paleoceanography 20, PA1003. https://doi.org/10.1029/2004PA001071

Liu, S., Jin, S., Liu, Y., Chen, A., 2022. Astronomical forced sequence infill of Early Cambrian Qiongzhusi organic-rich shale of Sichuan Basin, South China. Sediment. Geol. 440, 106261. https://doi.org/10.1016/j.sedgeo.2022.106261

Liu, W., Wu, H., Hinnov, L.A., Baddouh, M., Wang, P., Gao, Y., Zhang, S., Yang, T., Li, H., Wang, C., 2020. An 11 million-year-long record of astronomically forced fluvial-alluvial deposition and paleoclimate change in the Early Cretaceous Songliao synrift basin, China. Palaeogeogr. Palaeoclimatol. Palaeoecol. 541, 109555. https://doi.org/10.1016/j.palaeo.2019.109555

Liu, Y., Huang, C., Ogg, J.G., Algeo, T.J., Kemp, D.B., Shen, W., 2019. Oscillations of global sea-level elevation during the Paleogene correspond to 1.2-Myr amplitude modulation of orbital obliquity cycles. Earth Planet. Sci. Lett. 522, 65–78. https://doi.org/10.1016/j.epsl.2019.06.023

Liu, Z., Chen, Y., Yuan, L., 2001. The paleoclimate change of Qaidam Basin during the last 2.85 Ma recorded by Gamma-ray logging. Sci. China Ser. Earth Sci. 44, 133–145. https://doi.org/10.1007/BF02879656

Liu, Z., Huang, C., Algeo, T.J., Liu, H., Hao, Y., Du, X., Lu, Y., Chen, P., Guo, L., Peng, L., 2017. High-resolution astrochronological record for the Paleocene-Oligocene (66–23Ma) from the rapidly subsiding Bohai Bay Basin, northeastern China. Palaeogeogr. Palaeoclimatol. Palaeoecol. https://doi.org/10.1016/j.palaeo.2017.10.030

Locklair, R.E., Sageman, B.B., 2008. Cyclostratigraphy of the Upper Cretaceous Niobrara Formation, Western Interior, U.S.A.: A Coniacian–Santonian orbital timescale. Earth Planet. Sci. Lett. 269, 540–553. https://doi.org/10.1016/j.epsl.2008.03.021

Lofi, J., Voelker, A.H.L., Ducassou, E., Hernández-Molina, F.J., Sierro, F.J., Bahr, A., Galvani, A., Lourens, L.J., Pardo-Igúzquiza, E., Pezard, P., Rodríguez-Tovar, F.J., Williams, T., 2016. Quaternary chronostratigraphic framework and sedimentary processes for the Gulf of Cadiz and Portuguese Contourite Depositional Systems derived from Natural Gamma Ray records. Mar. Geol. 377, 40–57. https://doi.org/10.1016/j.margeo.2015.12.005

Ma, Y., Fan, M., Li, M., Ogg, J.G., Zhang, C., Feng, J., Zhou, C., Liu, X., Lu, Y., Liu, H., Eldrett, J.S., Ma, C., 2023. East Asian lake hydrology modulated by global sea-level variations in the Eocene warmhouse. Earth Planet. Sci. Lett. 602, 117925. https://doi.org/10.1016/j.epsl.2022.117925

MacLeod, K.G., White, L.T., Wainman, C.C., Martinez, M., Jones, M.M., Batenburg, S.J., Riquier, L., Haynes, S.J., Watkins, D.K., Bogus, K.A., Brumsack, H.-J., Guerra, R. do M., Edgar, K.M., Edvardsen, T., Harry, D.L., Hasegawa, T., Hobbs, R.W., Huber, B.T., Jiang, T., Kuroda, J., Lee, E.Y., Li, Y.-X., Maritati, A., O'Connor, L.K., Petrizzo, M.R., Quan, T.M., Richter, C., Tejada, M.L.G., Tagliaro, G., Wolfgring, E., Xu, Z., 2020. Late Cretaceous stratigraphy and paleoceanographic evolution in the Great Australian Bight Basin based on results from IODP Site U1512. Gondwana Res. 83, 80–95. https://doi.org/10.1016/j.gr.2020.01.009

Magnetic Susceptibility Sonde (MSS-B) [WWW Document], 2021. . Int. Ocean Discov. Program JOIDES Resolut. Sci. Oper. URL http://iodp.tamu.edu/tools/logging/SPECIAL/mss-b.html (accessed 6.24.21).

Makled, W.A., 2021. Applications of miospore quantitative stratigraphy and cyclostratigraphy in the Neocomian - Cenomanian sediments in the Western Desert, Egypt: A step in the way to biochronostratigraphy. Mar. Pet. Geol. 124, 104815. https://doi.org/10.1016/j.marpetgeo.2020.104815

Malinverno, A., Erba, E., Herbert, T.D., 2010. Orbital tuning as an inverse problem: Chronology of the early Aptian oceanic anoxic event 1a (Selli Level) in the Cismon APTICORE. Paleoceanography 25, PA2203. https://doi.org/10.1029/2009PA001769

Marković, S.B., Stevens, T., Kukla, G.J., Hambach, U., Fitzsimmons, K.E., Gibbard, P., Buggle, B., Zech, M., Guo, Z., Hao, Q., Wu, H., O'Hara Dhand, K., Smalley, I.J., Újvári, G., Sümegi, P., Timar-Gabor, A., Veres, D., Sirocko, F., Vasiljević, D.A., Jary, Z., Svensson, A., Jović, V., Lehmkuhl, F., Kovács, J., Svirčev, Z., 2015. Danube loess stratigraphy — Towards a pan-European loess stratigraphic model. Earth-Sci. Rev. 148, 228–258. https://doi.org/10.1016/j.earscirev.2015.06.005

Martinez, M., Deconinck, J.-F., Pellenard, P., Reboulet, S., Riquier, L., 2013. Astrochronology of the Valanginian Stage from reference sections (Vocontian Basin, France) and palaeoenvironmental implications for the Weissert Event. Palaeogeogr. Palaeoclimatol. Palaeoecol. 376, 91–102. https://doi.org/10.1016/j.palaeo.2013.02.021

Martinez, M., Kotov, S., De Vleeschouwer, D., Pas, D., Pälike, H., 2016. Testing the impact of stratigraphic uncertainty on spectral analyses of sedimentary series. Clim Past 12, 1765–1783. https://doi.org/10.5194/cp-12-1765-2016

Martinson, D.G., Menke, W., Stoffa, P., 1982. An inverse approach to signal correlation. J. Geophys. Res. Solid Earth 87, 4807–4818. https://doi.org/10.1029/JB087iB06p04807

Maurer, F., Hinnov, L., Schlager, W., 2004. Statistical time-series analysis and sedimentological tuning of bedding rhythms in a Triassic basinal succession (Southern Alps, Italy).

Melnyk, D.H., Smith, D.G., Amiri-Garroussi, K., 1994. Filtering and Frequency Mapping as Tools in Subsurface Cyclostratigraphy, with Examples from the Wessex Basin, UK, in: Orbital Forcing and Cyclic Sequences. John Wiley & Sons, Ltd, pp. 35–46. https://doi.org/10.1002/9781444304039.ch4

Meyers, S.R., 2019. Cyclostratigraphy and the problem of astrochronologic testing. Earth-Sci. Rev. 190, 190–223. https://doi.org/10.1016/j.earscirev.2018.11.015

Meyers, S.R., 2015. The evaluation of eccentricity-related amplitude modulation and bundling in paleoclimate data: An inverse approach for astrochronologic testing and time scale optimization. Paleoceanography 30, 1625–1640. https://doi.org/10.1002/2015PA002850

Meyers, S.R., 2014. astrochron: An R Package for Astrochronology Version 0.9.

Meyers, S.R., Sageman, B.B., 2007. Quantification of deep-time orbital forcing by average spectral misfit. Am. J. Sci. 307, 773–792. https://doi.org/10.2475/05.2007.01

Meyers, S.R., Siewert, S.E., Singer, B.S., Sageman, B.B., Condon, D.J., Obradovich, J.D., Jicha, B.R., Sawyer, D.A., 2012. Intercalibration of radioisotopic and astrochronologic time scales for the Cenomanian-Turonian boundary interval, Western Interior Basin, USA. Geology 40, 7–10. https://doi.org/10.1130/G32261.1

Milankovitch, M., 1941. Kanon der erdbestahlung und seine anwendung auf das eiszeitproblem, 133. K. Serbische Acad. Belgrade.

Molinie, A.J., Ogg, J.G., 1990. Sedimentation Rate Curves And Discontinuities From Sliding-window Spectral Analysis Of Logs. Log Anal. 31.

Morgans-Bell, H.S., Coe, A.L., Hessebo, S.P., Jenkyns, H.C., Weedon, G.P., Marshall, J.E.A., Tyson, R.V., Williams, C.J., 2001. Integrated stratigraphy of the Kimmeridge Clay Formation (Upper Jurassic) based on exposures and boreholes in south Dorset, UK. Geol. Mag. 138, 511–539. https://doi.org/10.1017/S0016756801005738

Muniz, M.C., Bosence, D.W.J., 2015. Pre-salt microbialites from the Campos Basin (offshore Brazil): image log facies, facies model and cyclicity in lacustrine carbonates. Geol. Soc. Lond. Spec. Publ. 418, 221–242. https://doi.org/10.1144/SP418.10

Necula, C., Dimofte, D., Panaiotu, C., 2015. Rock magnetism of a loess-palaeosol sequence from the western Black Sea shore (Romania). Geophys. J. Int. 202, 1733–1748. https://doi.org/10.1093/gji/ggv250

Niebuhr, B., Prokoph, A., 1997. Periodic-cyclic and chaotic successions of Upper Cretaceous (Cenomanian to Campanian) pelagic sediments in the North German Basin. Cretac. Res. 18, 731–750. https://doi.org/10.1006/cres.1997.0083

Niebuhr, B., Wiese, F., Wilmsen, M., 2001. The cored Konrad 101 borehole (Cenomanian–Lower Coniacian, Lower Saxony): calibration of surface and subsurface log data for the lower Upper Cretaceous of northern Germany. Cretac. Res. 22, 643–674. https://doi.org/10.1006/cres.2001.0283

Nio, S.D., Brouwer, J.H., Smith, D., de Jong, M., Böhm, A.R., 2005. Spectral trend attribute analysis: applications in the stratigraphic analysis of wireline logs. First Break 23.

Nowaczyk, N.R., 2001. Logging of Magnetic Susceptibility, in: Last, W.M., Smol, J.P. (Eds.), Tracking Environmental Change Using Lake Sediments: Basin Analysis, Coring, and Chronological Techniques. Springer Netherlands, Dordrecht, pp. 155–170. https://doi.org/10.1007/0-306-47669-X_8

Obreht, I., Wörmer, L., Brauer, A., Wendt, J., Alfken, S., De Vleeschouwer, D., Elvert, M., Hinrichs, K.-U., 2020. An annually resolved record of Western European vegetation response to Younger Dryas cooling. Quat. Sci. Rev. 231, 106198. https://doi.org/10.1016/j.quascirev.2020.106198

Ochoa, D., Sierro, F.J., Hilgen, F.J., Cortina, A., Lofi, J., Kouwenhoven, T., Flores, J.-A., 2018. Origin and implications of orbital-induced sedimentary cyclicity in Pliocene well-logs of the Western Mediterranean. Mar. Geol. 403, 150–164. https://doi.org/10.1016/j.margeo.2018.05.009

Ochoa, D., Sierro, F.J., Lofi, J., Maillard, A., Flores, J.-A., Suárez, M., 2015. Synchronous onset of the Messinian evaporite precipitation: First Mediterranean offshore evidence. Earth Planet. Sci. Lett. 427, 112–124. https://doi.org/10.1016/j.epsl.2015.06.059

Olsen, P.E., Laskar, J., Kent, D.V., Kinney, S.T., Reynolds, D.J., Sha, J., Whiteside, J.H., 2019. Mapping Solar System chaos with the Geological Orrery. Proc. Natl. Acad. Sci. 116, 10664–10673. https://doi.org/10.1073/pnas.1813901116

Paulissen, W.E., Luthi, S.M., 2011. High-frequency cyclicity in a Miocene sequence of the Vienna Basin established from high-resolution logs and robust chronostratigraphic tuning. Palaeogeogr. Palaeoclimatol. Palaeoecol. 307, 313–323. https://doi.org/10.1016/j.palaeo.2011.05.029

Peng, C., Zou, C., Zhang, S., Wu, H., Lü, Q., Hou, H., Wang, C., 2020. Astronomically forced variations in multiresolution resistivity logs of lower Upper Cretaceous (Cenomanian-Coniacian) terrestrial formations from the Songliao Basin, northeastern China. Palaeogeogr. Palaeoclimatol. Palaeoecol. 109858. https://doi.org/10.1016/j.palaeo.2020.109858

Perdiou, A., Thibault, N., Anderskouv, K., Buchem, F. van, Buijs, G.J.A., Bjerrum, C.J., 2016. Orbital calibration of the late Campanian carbon isotope event in the North Sea. J. Geol. Soc. 173, 504–517. https://doi.org/10.1144/jgs2015-120

Pierdominici, S., Kück, J., 2021. Borehole Geophysics, in: Alderton, D., Elias, S.A. (Eds.), Encyclopedia of Geology (Second Edition). Academic Press, Oxford, pp. 746–760. https://doi.org/10.1016/B978-0-08-102908-4.00126-0

Pierdominici, S., Millett, J.M., Kück, J.K.M., Thomas, D., Jerram, D.A., Planke, S., Haskins, E., Lautze, N., Galland, O., 2020. Stress Field Interactions Between Overlapping Shield Volcanoes: Borehole Breakout Evidence From the Island of Hawai'i, USA. J. Geophys. Res. Solid Earth 125, e2020JB019768. https://doi.org/10.1029/2020JB019768

Prokoph, A., Agterberg, F.P., 1999. Detection of sedimentary cyclicity and stratigraphic completeness by wavelet analysis; an application to late Albian cyclostratigraphy of the Western Canada Sedimentary Basin. J. Sediment. Res. 69, 862–875. https://doi.org/10.2110/jsr.69.862

Prokoph, A., Thurow, J., 2001. Orbital forcing in a 'Boreal' Cretaceous epeiric sea: high-resolution analysis of core and logging data (Upper Albian of the Kirchrode I drill core — Lower Saxony basin, NW Germany). Palaeogeogr. Palaeoclimatol. Palaeoecol. 174, 67–96. https://doi.org/10.1016/S0031-0182(01)00287-5

R Core Team, 2022. R: A Language and Environment for Statistical Computing.

Radke, B., Champion, D.C., Gallagher, S.J., Wang, L., De Vleeschouwer, D., Kalinowski, A., Tenthorey, E., Urosevic, M., Feitz, A., 2022. Geology, geochemistry and depositional history of the Port Campbell Limestone on the eastern flank of the Otway Basin, southeastern Australia. Aust. J. Earth Sci. 69, 509–538. https://doi.org/10.1080/08120099.2022.1998220

Radzevičius, S., Spiridonov, A., Brazauskas, A., 2014. Application of Wavelets to the Cyclostratigraphy of the Upper Homerian (Silurian) Gėluva Regional Stage in the Viduklė-61 Deep Well (Western Lithuania), in: Rocha, R., Pais, J., Kullberg, J.C., Finney, S. (Eds.), STRATI 2013. Springer International Publishing, Cham, pp. 437–440.

Radzevičius, S., Tumakovaitė, B., Spiridonov, A., 2017. Upper Homerian (Silurian) high-resolution correlation using cyclostratigraphy: an example from western Lithuania. Acta Geol. Pol. Vol. 67, no. 2, 307–322. https://doi.org/10.1515/agp-2017-0011

Rampino, M.R., Prokoph, A., Adler, A., 2000. Tempo of the end-Permian event: High-resolution cyclostratigraphy at the Permian-Triassic boundary. Geology 28, 643–646. https://doi.org/10.1130/0091-7613(2000)28<643:TOTEEH>2.0.CO;2

Read, J.F., Li, M., Hinnov, L.A., Nelson, C.S., Hood, S., 2020. Testing for astronomical forcing of cycles and gamma ray signals in outer shelf/upper slope, mixed siliciclastic-carbonates: Upper Oligocene, New Zealand. Palaeogeogr. Palaeoclimatol. Palaeoecol. 109821. https://doi.org/10.1016/j.palaeo.2020.109821

Reuning, L., Reijmer, J.J.G., Betzler, C., Timmermann, A., Steph, S., 2006. Sub-Milankovitch cycles in periplatform carbonates from the early Pliocene Great Bahama Bank. Paleoceanography 21. https://doi.org/10.1029/2004PA001075

Rider, M., Kennedy, M., 2011. The Geological Interpretation of Well Logs. published by Rider-French Consulting Ltd.

Rivera, T.A., Storey, M., Zeeden, C., Hilgen, F.J., Kuiper, K., 2011. A refined astronomically calibrated 40Ar/39Ar age for Fish Canyon sanidine. Earth Planet. Sci. Lett. 311, 420–426. https://doi.org/10.1016/j.epsl.2011.09.017

Ruffell, A., Worden, R., 2000. Palaeoclimate analysis using spectral gamma-ray data from the Aptian (Cretaceous) of southern England and southern France. Palaeogeogr. Palaeoclimatol. Palaeoecol. 155, 265–283. https://doi.org/10.1016/S0031-0182(99)00119-4

Russell, J.M., Bijaksana, S., Vogel, H., Melles, M., Kallmeyer, J., Ariztegui, D., Crowe, S., Fajar, S., Hafidz, A., Haffner, D., Hasberg, A., Ivory, S., Kelly, C., King, J., Kirana, K., Morlock, M., Noren, A., O'Grady, R., Ordonez, L., Stevenson, J., von Rintelen, T., Vuillemin, A., Watkinson, I., Wattrus, N., Wicaksono, S., Wonik, T., Bauer, K., Deino, A., Friese, A., Henny, C., Imran, Marwoto, R., Ngkoimani, L.O., Nomosatryo, S., Safiuddin, L.O., Simister, R., Tamuntuan, G., 2016. The Towuti Drilling Project: paleoenvironments, biological evolution, and geomicrobiology of a tropical Pacific lake. Sci. Drill. 21, 29–40. https://doi.org/10.5194/sd-21-29-2016

Russell, J.M., Vogel, H., Bijaksana, S., Melles, M., Deino, A., Hafidz, A., Haffner, D., Hasberg, A.K.M., Morlock, M., von Rintelen, T., Sheppard, R., Stelbrink, B., Stevenson, J., 2020. The late quaternary tectonic, biogeochemical, and environmental evolution of ferruginous Lake Towuti, Indonesia. Palaeogeogr. Palaeoclimatol. Palaeoecol. 556, 109905. https://doi.org/10.1016/j.palaeo.2020.109905

Sacchi, M., Müller, P., 2004. Orbital cyclicity and astronomical calibration of the Upper Miocene continental succession cored at the Iharosbereny-I well site, Western Pannonian basin, Hungary.

Sardar Abadi, M., Zeeden, C., Ulfers, A., Wonik, T., 2022. An astronomical age-depth model and reconstruction of moisture availability in the sediments of Lake Chalco, central Mexico, using borehole logging data. Quat. Sci. Rev. 294, 107739. https://doi.org/10.1016/j.quascirev.2022.107739

Schlumberger, 2013. Log Interpretation Charts.

Schnyder, J., Ruffell, A., Deconinck, J.-F., Baudin, F., 2006. Conjunctive use of spectral gamma-ray logs and clay mineralogy in defining late Jurassic–early Cretaceous palaeoclimate change (Dorset, U.K.). Palaeogeogr. Palaeoclimatol. Palaeoecol. 229, 303–320. https://doi.org/10.1016/j.palaeo.2005.06.027

Shackleton, N.J., Crowhurst, S.J., Weedon, G.P., Laskar, J., 1999. Astronomical calibration of Oligocene--Miocene time. Philos. Trans. R. Soc. Lond. Ser. Math. Phys. Eng. Sci. 357, 1907–1929. https://doi.org/10.1098/rsta.1999.0407

Shackleton, N.J., Hagelberg, T.K., Crowhurst, S.J., 1995. Evaluating the success of astronomical tuning: Pitfalls of using coherence as a criterion for assessing pre-Pleistocene timescales. Paleoceanography 10, 693–697. https://doi.org/10.1029/95PA01454

Shi, J., Jin, Z., Liu, Q., Zhang, R., Huang, Z., 2019. Cyclostratigraphy and astronomical tuning of the middle eocene terrestrial successions in the Bohai Bay Basin, Eastern China. Glob. Planet. Change 174, 115–126. https://doi.org/10.1016/j.gloplacha.2019.01.001

Shifeng, T., Zhongqiang, C., Chunju, H., Changhai, G., Ming, Z., 2013. Astronomical Dating of the Middle Miocene Hanjiang Formation in the Pearl River Mouth Basin, South China Sea. Acta Geol. Sin. - Engl. Ed. 87, 48–58. https://doi.org/10.1111/1755-6724.12029

Sierro, F.J., Ledesma, S., Flores, J.-A., Torrescusa, S., Olmo, W.M. del, 2000. Sonic and gamma-ray astrochronology: Cycle to cycle calibration of Atlantic climatic records to Mediterranean sapropels and astronomical oscillations. Geology 28, 695–698. https://doi.org/10.1130/0091-7613(2000)28<695:SAGACT>2.0.CO;2

Sinnesael, M., McLaughlin, P.I., Desrochers, A., Mauviel, A., De Weirdt, J., Claeys, P., Vandenbroucke, T.R.A., 2021. Precession-driven climate cycles and time scale prior to the Hirnantian glacial maximum. Geology 49, 1295–1300. https://doi.org/10.1130/G49083.1

Szabó, N.P., Nehéz, K., Hornyák, O., Piller, I., Deák, Cs., Hanzelik, P.P., Kutasi, Cs., Ott, K., 2019. Cluster analysis of core measurements using heterogeneous data sources: An application to complex Miocene reservoirs. J. Pet. Sci. Eng. 178, 575–585. https://doi.org/10.1016/j.petrol.2019.03.067

Tang, Y., Zheng, M., Wang, X., Wang, T., Cheng, H., Hei, C., 2022. The floating astronomical time scale for the terrestrial Early Permian Fengcheng Formation from the Junggar Basin and its stratigraphic and palaeoclimate implications. Geol. J. 57, 4842–4856. https://doi.org/10.1002/gj.4575

Telford, R.J., Heegaard, E., Birks, H.J.B., 2004. All age–depth models are wrong: but how badly? Quat. Sci. Rev. 23, 1–5. https://doi.org/10.1016/j.quascirev.2003.11.003

Tiedemann, R., Haug, G.H., 1992. 19. ASTRONOMICAL CALIBRATION OF CYCLE STRATIGRAPHY FOR SITE 882 IN THE NORTHWEST PACIFIC1.

Trachsel, M., Telford, R.J., 2017. All age–depth models are wrong, but are getting better. The Holocene 27, 860–869. https://doi.org/10.1177/0959683616675939

Trauth, M.H., Gebbers, R., Marwan, N., Sillmann, E., 2007. MATLAB recipes for earth sciences. Springer.

Trauth, M.H., Larrasoaña, J.C., Mudelsee, M., 2009. Trends, rhythms and events in Plio-Pleistocene African climate. Quat. Sci. Rev. 28, 399–411. https://doi.org/10.1016/j.quascirev.2008.11.003

Trice, R., 1999. A methodology for applying a non unique, morphological classification to sine wave events picked from borehole image log data. Geol. Soc. Lond. Spec. Publ. 159, 77–90. https://doi.org/10.1144/GSL.SP.1999.159.01.04

Turtù, A., Lauretano, V., Catanzariti, R., Hilgen, F.J., Galeotti, S., Lanci, L., Moretti, M., Lourens, L.J., 2017. Integrated stratigraphy of the Smirra Core (Umbria-Marche Basin, Apennines, Italy): A new early Paleogene reference section and implications for the geologic time scale. Palaeogeogr. Palaeoclimatol. Palaeoecol. 487, 158–174. https://doi.org/10.1016/j.palaeo.2017.08.031

Ulfers, A., Hesse, K., Zeeden, C., Russell, J.M., Vogel, H., Bijaksana, S., Wonik, T., 2021. Cyclostratigraphy and paleoenvironmental inference from downhole logging of sediments in tropical Lake Towuti, Indonesia. J. Paleolimnol. https://doi.org/10.1007/s10933-020-00171-9

Ulfers, A., Zeeden, C., Voigt, S., Sardar Abadi, M., Wonik, T., 2022a. Half-precession signals in Lake Ohrid (Balkan) and their spatio-temporal relations to climate records from the European realm. Quat. Sci. Rev. 280, 107413. https://doi.org/10.1016/j.quascirev.2022.107413

Ulfers, A., Zeeden, C., Wagner, B., Krastel, S., Buness, H., Wonik, T., 2022b. Borehole logging and seismic data from Lake Ohrid (North Macedonia/Albania) as a basis for age-depth modelling over the last one million years. Quat. Sci. Rev. 276, 107295. https://doi.org/10.1016/j.quascirev.2021.107295

Vaucher, R., Dashtgard, S.E., Horng, C.-S., Zeeden, C., Dillinger, A., Pan, Y.-Y., Setiaji, R.A., Chi, W.-R., Löwemark, L., 2021. Insolation-paced sea level and sediment flux during the early Pleistocene in Southeast Asia. Sci. Rep. 11, 16707. https://doi.org/10.1038/s41598-021-96372-x

Vinnepand, M., Fischer, P., Jöris, O., Hambach, U., Zeeden, C., Schulte, P., Fitzsimmons, K.E., Prud'homme, C., Perić, Z., Schirmer, W., Lehmkuhl, F., Fiedler, S., Vött, A., 2022. Decoding geochemical signals of the Schwalbenberg Loess-Palaeosol-Sequences — A key to Upper Pleistocene ecosystem responses to climate changes in western Central Europe. CATENA 212, 106076. https://doi.org/10.1016/j.catena.2022.106076

Vogel, H., Wagner, B., Zanchetta, G., Sulpizio, R., Rosén, P., 2010. A paleoclimate record with tephrochronological age control for the last glacial-interglacial cycle from Lake Ohrid, Albania and Macedonia. J. Paleolimnol. 44, 295–310. https://doi.org/10.1007/s10933-009-9404-x

Voigt, S., Erbacher, J., Mutterlose, J., Weiss, W., Westerhold, T., Wiese, F., Wilmsen, M., Wonik, T., 2008. The Cenomanian – Turonian of the Wunstorf section – (North Germany): global stratigraphic reference section and new orbital time scale for Oceanic Anoxic Event 2. Newsl. Stratigr. 43, 65–89. https://doi.org/10.1127/0078-0421/2008/0043-0065

Wagner, B., Wilke, T., Krastel, S., Zanchetta, G., Sulpizio, R., Reicherter, K., Leng, M.J., Grazhdani, A., Trajanovski, S., Francke, A., Lindhorst, K., Levkov, Z., Cvetkoska, A., Reed, J.M., Zhang, X., Lacey, J.H., Wonik, T., Baumgarten, H., Vogel, H., 2014. The SCOPSCO drilling project recovers more than 1.2 million years of history from Lake Ohrid. Sci. Drill. 17, 19–29. https://doi.org/10.5194/sd-17-19-2014

Wang, M., Chen, H., Huang, C., Kemp, D.B., Xu, T., Zhang, H., Li, M., 2020. Astronomical forcing and sedimentary noise modeling of lake-level changes in the Paleogene Dongpu Depression of North China. Earth Planet. Sci. Lett. 535, 116116. https://doi.org/10.1016/j.epsl.2020.116116

Wang, M., Li, M., Kemp, D.B., Boulila, S., Ogg, J.G., 2022. Sedimentary noise modeling of lake-level change in the Late Triassic Newark Basin of North America. Glob. Planet. Change 208, 103706. https://doi.org/10.1016/j.gloplacha.2021.103706

Wang, Xuetian, Shao, L., Eriksson, K.A., Yan, Z., Wang, J., Li, H., Zhou, R., Lu, J., 2020. Evolution of a plume-influenced source-to-sink system: An example from the coupled central Emeishan large igneous province and adjacent western Yangtze cratonic basin in the Late Permian, SW China. Earth-Sci. Rev. 207, 103224. https://doi.org/10.1016/j.earscirev.2020.103224

Wang, Xiuqi, Zhang, X., Gao, F., Zhang, M., 2020. Astronomical Cycles of the Late Permian Lopingian in South China and Their Implications for Third-Order Sea-Level Change. J. Ocean Univ. China 19, 1331–1344. https://doi.org/10.1007/s11802-020-4438-9

Wang, Z., Mao, Y., Geng, J., Huang, C., Ogg, J., Kemp, D.B., Zhang, Z., Pang, Z., Zhang, R., 2022. Pliocene-Pleistocene evolution of the lower Yellow River in eastern North China: Constraints on the age of the Sanmen Gorge connection. Glob. Planet. Change 213, 103835. https://doi.org/10.1016/j.gloplacha.2022.103835

Weatherford, 2007. Wireline Services Log InterpretationChart Book.

Weedon, G.P., 2022. Problems with the current practice of spectral analysis in cyclostratigraphy: Avoiding false detection of regular cyclicity. Earth-Sci. Rev. 235, 104261. https://doi.org/10.1016/j.earscirev.2022.104261

Weedon, G.P., 2003. Time-Series Analysis and Cyclostratigraphy: Examining Stratigraphic Records of Environmental Cycles. Cambridge University Press.

Weedon, G.P., Coe, A.L., Gallois, R.W., 2004. Cyclostratigraphy, orbital tuning and inferred productivity for the type Kimmeridge Clay (Late Jurassic), Southern England. J. Geol. Soc. 161, 655–666. https://doi.org/10.1144/0016-764903-073

Weedon, G.P., Jenkyns, H.C., Coe, A.L., Hesselbo, S.P., 1999. Astronomical calibration of the Jurassic time-scale from cyclostratigraphy in British mudrock formations. Philos. Trans. R. Soc. Lond. Ser. Math. Phys. Eng. Sci. 357, 1787–1813. https://doi.org/10.1098/rsta.1999.0401

Wei, W., Lu, Y., Xing, F., Liu, Z., Pan, L., Algeo, T.J., 2017. Sedimentary facies associations and sequence stratigraphy of source and reservoir rocks of the lacustrine Eocene Niubao Formation (Lunpola

Basin, central Tibet). Mar. Pet. Geol. 86, 1273–1290. https://doi.org/10.1016/j.marpetgeo.2017.07.032

Wilke, T., Wagner, B., Van Bocxlaer, B., Albrecht, C., Ariztegui, D., Delicado, D., Francke, A., Harzhauser, M., Hauffe, T., Holtvoeth, J., Just, J., Leng, M.J., Levkov, Z., Penkman, K., Sadori, L., Skinner, A., Stelbrink, B., Vogel, H., Wesselingh, F., Wonik, T., 2016. Scientific drilling projects in ancient lakes: Integrating geological and biological histories. Glob. Planet. Change 143, 118–151. https://doi.org/10.1016/j.gloplacha.2016.05.005

Wilkens, R., Westerhold, T., Drury, A.J., Lyle, M., Gorgas, T., Tian, J., 2017. Revisiting the Ceara Rise, equatorial Atlantic Ocean: isotope stratigraphy of ODP Leg 154. Clim. Past 2017, 1–22. https://doi.org/10.5194/cp-2016-140

Williams, T., Kroon, D., Spezzaferri, S., 2002. Middle and Upper Miocene cyclostratigraphy of downhole logs and short- to long-term astronomical cycles in carbonate production of the Great Bahama Bank. Mar. Geol. 185, 75–93. https://doi.org/10.1016/S0025-3227(01)00291-2

Williams, T., Pirmez, C., 1999. FMS Images from carbonates of the Bahama Bank Slope, ODP Leg 166: Lithological identification and cyclo-stratigraphy. Geol. Soc. Lond. Spec. Publ. 159, 227–238. https://doi.org/10.1144/GSL.SP.1999.159.01.12

Wonik, T., 2001. Gamma-ray measurements in the Kirchrode I and II boreholes. Palaeogeogr. Palaeoclimatol. Palaeoecol. 174, 97–105. https://doi.org/10.1016/S0031-0182(01)00288-7

Worthington, P.F., 1990. Sediment cyclicity from well logs. Geol. Soc. Lond. Spec. Publ. 48, 123–132. https://doi.org/10.1144/GSL.SP.1990.048.01.11

Wu, H., Hinnov, L.A., Zhang, S., Jiang, G., Yang, T., Li, H., Xi, D., Ma, X., Wang, C., 2022. Continental geological evidence for Solar System chaotic behavior in the Late Cretaceous. GSA Bull. https://doi.org/10.1130/B36340.1

Wu, H., Zhang, S., Hinnov, L.A., Jiang, G., Yang, T., Li, H., Wan, X., Wang, C., 2014. Cyclostratigraphy and orbital tuning of the terrestrial upper Santonian–Lower Danian in Songliao Basin, northeastern China. Earth Planet. Sci. Lett. 407, 82–95. https://doi.org/10.1016/j.epsl.2014.09.038

WU, H., ZHANG, S., HUANG, Q., 2008. Establishment of Floating Astronomical Time Scale for the Terrestrial Late Cretaceous Qingshankou Formation in the Songliao Basin of Northeast China. Earth Sci. Front. 15, 159–169. https://doi.org/10.1016/S1872-5791(08)60049-4

Wu, H., Zhang, S., Jiang, G., Hinnov, L., Yang, T., Li, H., Wan, X., Wang, C., 2013. Astrochronology of the Early Turonian–Early Campanian terrestrial succession in the Songliao Basin, northeastern China and its implication for long-period behavior of the Solar System. Palaeogeogr. Palaeoclimatol. Palaeoecol., Environmental/Climate Change in the Cretaceous Greenhouse World: records from terrestrial scientific drilling of Songliao Basin and adjacent area of China 385, 55–70. https://doi.org/10.1016/j.palaeo.2012.09.004

Wu, H., Zhang, S., Jiang, G., Huang, Q., 2009. The floating astronomical time scale for the terrestrial Late Cretaceous Qingshankou Formation from the Songliao Basin of Northeast China and its stratigraphic and paleoclimate implications. Earth Planet. Sci. Lett. 278, 308–323. https://doi.org/10.1016/j.epsl.2008.12.016

WU, H., Zhang, S., Sui, S., Huang, Q., 2007. Recognition of Milankovitch Cycles in the Natural Gamma–Ray Logging of Upper Cretaceous Terrestrial Strata in the Songliao Basin. Acta Geol. Sin. - Engl. Ed. 81, 996–1001. https://doi.org/10.1111/j.1755-6724.2007.tb01021.x

Xia, S., Lin, C., Du, X., Jia, D., Ahmad, N., Zhang, Z., Gao, L., Zhu, Y., 2020. Correspondences among lacustrine fluctuations, climate changes and the Milankovitch cycles in the Paleogene through tracking onlap points and correlating palaeontology in Liaozhong Depression, Bohai Bay Basin, NE China. Geol. J. 55, 6527–6543. https://doi.org/10.1002/gj.3825

Xu, K., Chen, H., Huang, C., Ogg, J.G., Zhu, J., Lin, S., Yang, D., Zhao, P., Kong, L., 2019. Astronomical time scale of the Paleogene lacustrine paleoclimate record from the Nanxiang Basin, central China. Palaeogeogr. Palaeoclimatol. Palaeoecol. 532, 109253. https://doi.org/10.1016/j.palaeo.2019.109253

Yang, C.S., Baumfalk, Y.A., 1994. Milankovitch Cyclicity in the Upper Rotliegend Group of The Netherlands Offshore, in: Orbital Forcing and Cyclic Sequences. John Wiley & Sons, Ltd, pp. 47–61. https://doi.org/10.1002/9781444304039.ch5

Yang, S., Ding, Z., 2014. A 249 kyr stack of eight loess grain size records from northern China documenting millennial-scale climate variability. Geochem. Geophys. Geosystems 15, 798–814. https://doi.org/10.1002/2013GC005113

Yi, L., Shi, Z., Tan, L., Deng, C., 2017. Orbital-scale nonlinear response of East Asian summer monsoon to its potential driving forces in the late Quaternary. Clim. Dyn. 1–15. https://doi.org/10.1007/s00382-017-3743-5

YU, J., SUI, F., LI, Z., LIU, H., WANG, Y., 2008. Recognition of Milankovitch cycles in the stratigraphic record: application of the CWT and the FFT to well-log data. J. China Univ. Min. Technol. 18, 594–598. https://doi.org/10.1016/S1006-1266(08)60301-6

Yuan, R., Zhu, R., Xie, S., Hu, W., Zhou, F., Yu, Y., 2019. Utilizing Maximum Entropy Spectral Analysis (MESA) to identify Milankovitch cycles in Lower Member of Miocene Zhujiang Formation in north slope of Baiyun Sag, Pearl River Mouth Basin, South China Sea. Open Geosci. 11, 877–887. https://doi.org/doi:10.1515/geo-2019-0068

Zeeden, C., Dietze, M., Kreutzer, S., 2018a. Discriminating luminescence age uncertainty composition for a robust Bayesian modelling. Quat. Geochronol. 43, 30–39. https://doi.org/10.1016/j.quageo.2017.10.001

Zeeden, C., Hambach, U., Obreht, I., Hao, Q., Abels, H.A., Veres, D., Lehmkuhl, F., Gavrilov, M.B., Marković, S.B., 2018b. Patterns and timing of loess-paleosol transitions in Eurasia: Constraints for paleoclimate studies. Glob. Planet. Change 162, 1–7. https://doi.org/10.1016/j.gloplacha.2017.12.021

Zeeden, C., Hilgen, F., Westerhold, T., Lourens, L., Röhl, U., Bickert, T., 2013. Revised Miocene splice, astronomical tuning and calcareous plankton biochronology of ODP Site 926 between 5 and 14.4 Ma. Palaeogeogr. Palaeoclimatol. Palaeoecol. 369, 430–451. https://doi.org/10.1016/j.palaeo.2012.11.009

Zeeden, C., Kaboth, S., Hilgen, F.J., Laskar, J., 2018c. Taner filter settings and automatic correlation optimisation for cyclostratigraphic studies. Comput. Geosci. 119, 18–28. https://doi.org/10.1016/j.cageo.2018.06.005

Zeeden, C., Kels, H., Hambach, U., Schulte, P., Protze, J., Eckmeier, E., Marković, S.B., Klasen, N., Lehmkuhl, F., 2016. Three climatic cycles recorded in a loess-palaeosol sequence at Semlac (Romania) – Implications for dust accumulation in south-eastern Europe. Quat. Sci. Rev. 154, 130–142. https://doi.org/10.1016/j.quascirev.2016.11.002

Zeeden, C., Meyers, S.R., Hilgen, F.J., Lourens, L.J., Laskar, J., 2019. Time scale evaluation and the quantification of obliquity forcing. Quat. Sci. Rev. 209, 100–113. https://doi.org/10.1016/j.quascirev.2019.01.018

Zeeden, C., Meyers, S.R., Lourens, L.J., Hilgen, F.J., 2015. Testing astronomically tuned age models. Paleoceanography 30, 2014PA002762. https://doi.org/10.1002/2014PA002762

Zemanek, J., Caldwell, R.L., Glenn, E.E., Holcomb, S.V., Norton, L.J., Straus, A.J.D., 1969. The borehole televiewera new logging concept for fracture location and other types of borehole inspection. J. Pet. Technol. 21, 762–774.

Zhang, J., Pas, D., Krijgsman, W., Wei, W., Du, X., Zhang, C., Liu, J., Lu, Y., 2020. Astronomical forcing of the Paleogene coal-bearing hydrocarbon source rocks of the East China Sea Shelf Basin. Sediment. Geol. 406, 105715. https://doi.org/10.1016/j.sedgeo.2020.105715

Zhang, R., Li, L., Nai, W., Gu, Y., Huang, C., Ogg, J., Li, Q., Lu, C., Wang, Z., 2019. Astronomical forcing of terrestrial climate recorded in the Pleistocene of the western Tarim Basin, NW China. Palaeogeogr. Palaeoclimatol. Palaeoecol. 530, 78–89. https://doi.org/10.1016/j.palaeo.2019.05.039

Zhang, T., Li, Y., Fan, T., Silva, A.-C.D., Shi, J., Gao, Q., Kuang, M., Liu, W., Gao, Z., Li, M., 2022. Orbitally-paced climate change in the early Cambrian and its implications for the history of the Solar System. Earth Planet. Sci. Lett. 583, 117420. https://doi.org/10.1016/j.epsl.2022.117420

Zhang, T., Zhang, C., Fan, T., Zhang, L., Zhu, R., Tao, J., Li, M., 2020. Cyclostratigraphy of Lower Triassic terrestrial successions in the Junggar Basin, northwestern China. Palaeogeogr. Palaeoclimatol. Palaeoecol. 539, 109493. https://doi.org/10.1016/j.palaeo.2019.109493

**Figures and Table:**

**Table 1:** Extensive overview on studies using borehole logging data for cyclostratigraphy. While most of the cited studies here apply cyclostratigraphy, few focus on technical/computational aspects.

| Type of downhole logging data | Formation/Location | Age | Reference |
|---|---|---|---|
| Conductivity log | Meuse/Haute-Marne, France | Upper Jurassic | (Lefranc et al., 2008) |
| Electrical Image Log | Vienna Basin, Austria | Miocene | (Lai et al., 2018) |
| Formation MicroImager resistivity log | ODP Leg 166, SE of Florida/USA | Miocene | (Williams et al., 2002) |
| Formation MicroImager tools | Niobrara Formation, USA | Upper Cretaceous | (Locklair and Sageman, 2008) |
| Formation MicroScanner log | ODP Site 978B, Mediterranean | Quaternary | (Goldberg, 1997) |
| Formation MicroScanner log | Kimmeridge Clay Formation, UK | Late Jurassic | (Huang et al., 2010) |
| Formation MicroScanner, Resistivity logs | Cismon Valley, northern Italy | Cretaceous | (Malinverno et al., 2010) |
| Gamma ray log | Foz do Amazonas Basin, Brazil | Cretaceous | (Boulila et al., 2020) |
| Gamma ray log | South China Sea | Eocene | (Cao et al., 2016) |
| Gamma ray log | Gulf of Suez, Egypt | Miocene | (Farouk et al., 2022a) |
| Gamma ray log | Bohai Basin, China | Paleogene | (Xia et al., 2020) |
| Gamma ray log | Pinghu Formation, China | Paleogene | (J. Zhang et al., 2020) |
| Gamma ray log | Mediterranean, Egypt | Pliocene | (Farouk et al., 2022b) |
| Gamma ray log | Lake Ohrid, Balkan | Quaternary | (Baumgarten et al., 2015; Ulfers et al., 2022b) |
| Gamma ray and Density logs | Juggar Basin, China | Permian | (Tang et al., 2022) |
| Gamma ray and Density logs | Zakeen Formation, Persian Gulf | Devonian | (Falahatkhah et al., 2020) |
| Gamma ray and Density logs, Sonic transit time | Dalan Formation, Persian Gulf | Late Permian | (Falahatkhah et al., 2021b, 2021a) |
| Gamma Ray and Neutron logs | Paradox Basin strata, USA | Carboniferous | (Goldhammer et al., 1994) |
| Gamma ray and Sonic velocity logs | Green River Formation, USA | Eocene | (Fischer and Roberts, 1991) |
| Gamma ray and Sonic velocity logs | Rotliegend Group offshore, Netherlands | Permian | (Yang and Baumfalk, 1994) |
| Gamma ray log | Western Canada Basin, Canada | Albian, Cretaceous | (Prokoph and Agterberg, 1999) |

| | | | |
|---|---|---|---|
| Gamma ray log | Qiongzhusi Formation, Chengdu, China | Cambrian | (Liu et al., 2022; Zhang et al., 2022) |
| Gamma ray log | ODP Site 549, North Atlantic | Cretaceous | (Kouamelan et al., 2021) |
| Gamma ray log | North Sea | Cretaceous | (Perdiou et al., 2016) |
| Gamma ray log | IODP Site U1512, Australian Bight Basion | Cretaceous | (MacLeod et al., 2020) |
| Gamma ray log | Western Desert, Egypt | Cretaceous | (Makled, 2021) |
| Gamma ray log | Lower Saxonian Basin, Germany | Cretaceous | (Voigt et al., 2008) |
| Gamma ray log | Fiq Formation, Oman | Cryogenian | (Gong, 2021) |
| Gamma ray log | Albian claystone of Herbram Formation, Germany | Early Cretaceous | (Prokoph and Thurow, 2001; Wonik, 2001) |
| Gamma ray log | Nafun & Ara Group, Oman | Ediacarian | (Gong and Li, 2020) |
| Gamma ray log | Jianghan Basin, China | Eocene-Oligocene | (Huang and Hinnov, 2019) |
| Gamma ray log | Rennes Basin, France | Eocene–Oligocene | (Boulila et al., 2021) |
| Gamma ray log | Tikorangi Formation, New Zealand | Late Oligocene | (Read et al., 2020) |
| Gamma ray log | Qiangtang Basin, China | Middle Jurassic | (Gao et al., 2020) |
| Gamma ray log | Ordos Basin, China | Middle Jurassic | (Chen et al., 2022) |
| Gamma ray log | Otway Basin, Australia | Miocene | (Radke et al., 2022) |
| Gamma ray log | South China Sea | Miocene | (Shifeng et al., 2013; Yuan et al., 2019) |
| Gamma ray log | Bohai Basin, China | Oligocene | (Du et al., 2020) |
| Gamma ray log | Tarim Basin, China | Ordovician | (Aboubacar et al., 2022) |
| Gamma ray log | Sichuan Basin, China | Ordovician-Silurian | (Lang et al., 2018) |
| Gamma ray log | Bohai Bay Basin, China | Paleocene-Oligocene | (Liu et al., 2017) |
| Gamma ray log | Lishui Depression, China | Paleogene | (Liu et al., 2019) |
| Gamma ray log | Shahejie Formation, Dongpu & Dongying Depressions, China | Paleogene | (Ma et al., 2023; M. Wang et al., 2020) |
| Gamma ray log | Nanxiang Basin, China | Paleogene | (Xu et al., 2019) |

| | | | |
|---|---|---|---|
| Gamma ray log | Paraná Basin, Brazil | Permian | (Fritzen et al., 2019) |
| Gamma ray log | Yangtze cratonic basin, China | Permian | (Xuetian Wang et al., 2020) |
| Gamma ray log | North Sea | Permian | (Nio et al., 2005) |
| Gamma ray log | Pingle Depression, China | Permian | (Xiuqi Wang et al., 2020) |
| Gamma ray log | China | Permo-carboniferous | (YU et al., 2008) |
| Gamma ray log | Taiyuan Basin, China | Plio-Pleistocene | (Z. Wang et al., 2022) |
| Gamma ray log | IODP Site U1463, Offshore NW Australia | Plio-Pleistocene | (Christensen et al., 2017) |
| Gamma ray log | Quaidam Basin, China | Plio-Pleistocene | (Liu et al., 2001) |
| Gamma ray log | Lake Chalco, Mexico | Quaternary | (Brown et al., 2019) |
| Gamma ray log | Lake Chalco, Mexico | Quaternary | (Sardar Abadi et al., 2022) |
| Gamma ray log | lleung Basin, East Sea | Quaternary | (Bahk et al., 2016) |
| Gamma ray log | Gulf of Cadiz/Portugal | Quaternary | (Lofi et al., 2016) |
| Gamma ray log | Coastal Plain of Israel | Permian-Triassic | (Korngreen et al., 2013) |
| Gamma ray log | Lithuania | Silurian | (Radzevičius et al., 2014, 2017) |
| Gamma ray log | Buchstein, Italy | Triassic | (Maurer et al., 2004) |
| Gamma ray log | Bohemian Cretaceous Basin, Czech Republic | Turonian-Coniacian | (Laurin et al., 2014; Laurin and Uličn;ý, 2004) |
| Gamma ray log | Wessex Basin, UK | Upper Jurassic | (Melnyk et al., 1994) |
| Gamma ray log | Anticosti Island, Canada | Ordovician | (Sinnesael et al., 2021) |
| Gamma ray log | Franconian and Swabian Alb, Germany | Middle Jurassic | (Leu et al., 2022) |
| Gamma ray and Density logs | Tarfaya Basin, Morocco | Cenomanian/Turonian | (Beil et al., 2020, 2018; Kuhnt et al., 1997) |
| Gamma ray and Density logs | Carnic Alps in Austria | Permian-Triassic | (Rampino et al., 2000) |
| Gamma ray and Formation MicroImager resistivity logs | Vienna Basin, Austria | Miocene | (Paulissen and Luthi, 2011) |
| Gamma ray and Magnetic susceptibility logs | Bohai Basin, China | Eocene | (Guo and Jin, 2021; Jin et al., 2022; Shi et al., 2019) |
| Gamma ray and Magnetic susceptibility logs | Tarim Basin, China | Pleistocene | (Zhang et al., 2019) |
| Gamma ray and Resistivity logs | Buqu Formation, Tibet, China | Middle Jurassic | (Cheng et al., 2017) |
| Gamma ray, Resistivity and Sonic velocity logs | Western Mediterranean | Miocene, Pliocene | (Ochoa et al., 2015) |

| | | | |
|---|---|---|---|
| Gamma ray, Resistivity, Sonic velocity logs | Western Mediterranean | Pliocene | (Ochoa et al., 2018) |
| Gamma ray and Sonic velocity logs | Lunpola Basin, Tibet, China | Eocene | (Wei et al., 2017) |
| Gamma ray, Caliper, Density logs | Juggar Basin, China | Carboniferous-Permian | (Huang et al., 2021) |
| Gamma ray and Density logs | Songliao Basin Transect, China | Cwenomanian-Coniacian | (Wu et al., 2009) |
| Gamma ray, Formation MicroScanner logs | Kimmeridge Clay, UK | Late Jurassic | (Huang et al., 2010; Morgans-Bell et al., 2001) |
| Gamma ray, Magnetic susceptibility, Resistivity and Density logs | Songliao Basin, China | Cretaceous | (Liu et al., 2020; Peng et al., 2020; WU et al., 2008; Wu et al., 2013, 2014; Li et al., 2022; Wu et al., 2022; WU et al., 2007) |
| Gamma ray, Porosity, Sonic velocity logs | Ocean Drilling Program, Leg 105, Labrador Sea and Baffin Bay | Pliocene – Pleistocene | (Jarrard and Arthur, 1989) |
| Gamma ray, Resistivity and Density logs | Juggar Basin, China | Jurassic | (Y. Li et al., 2018) |
| Gamma ray and Resistivity logs | Ocean Drilling Program Sites 865 and 866, western Pacific Ocean | Late Albian, Early Cretaceous | (Cooper, 1995) |
| Gamma ray and Resistivity logs | Gulf of Cadiz/Portugal | Miocene-Pleistocene | (Hernández-Molina et al., 2016) |
| Gamma ray and Sonic velocity logs | Gulf of Cadiz, Portugal/Spain | Pliocene | (Sierro et al., 2000) |
| Gamma ray and Sonic velocity logs | Newark–Hartford Basins, USA | Triassic | (Olsen et al., 2019; M. Wang et al., 2022) |
| Induction log | ODP site 646B, Labrador Sea | Pliocene | (Worthington, 1990) |
| Magnetic susceptibility log | North Sea | Plio-Pleistocene | (Barthès et al., 1999) |
| Magnetic susceptibility log | Meuse, France | Jurassic | (Huret et al., 2011) |
| Magnetic susceptibility log | Kimmeridge Clay Formation, UK | Late Jurassic | (Weedon et al., 1999) |
| Magnetic susceptibility log | Lake Towuti, Indonesia | Quaternary | (Ulfers et al., 2021) |
| Magnetic susceptibility and Density logs | Ocean Drilling Program Site 882, north west Pacific Ocean | Pliocene | (Tiedemann and Haug, 1992) |
| Magnetic susceptibility, Formation MicroImager resistivity logs | ODP Leg 166, SE of Florida/USA | Pliocene | (Kroon et al., 2000) |
| Photoelectric Effect and Gamma ray logs | Kimmeridge Clay Formation, UK | Late Jurassic | (Weedon et al., 2004) |

| | | | |
|---|---|---|---|
| Resistivity log | Lower Saxony Basin, Germany | Cenomanian–Lower Coniacian | (Niebuhr et al., 2001) |
| Resistivity log | ODP Site 1006, SE of Florida/USA | Pliocene | (Reuning et al., 2006) |
| Resistivity and Sonic velocity logs | ODP Site 963, Weddell Sea | Paleogene to Pliocene | (Golovchenko et al., 1990) |
| Resistivity and Spontaneous potential logs | Pannonian Basin, Hungary | Miocene | (Sacchi and Müller, 2004) |
| Self potential logs | North German Basin, Germany | Cretaceous | (Niebuhr and Prokoph, 1997) |
| U concentration, based on Gamma ray log | Lake Van, Turkey | Quaternary | (Baumgarten and Wonik, 2015) |

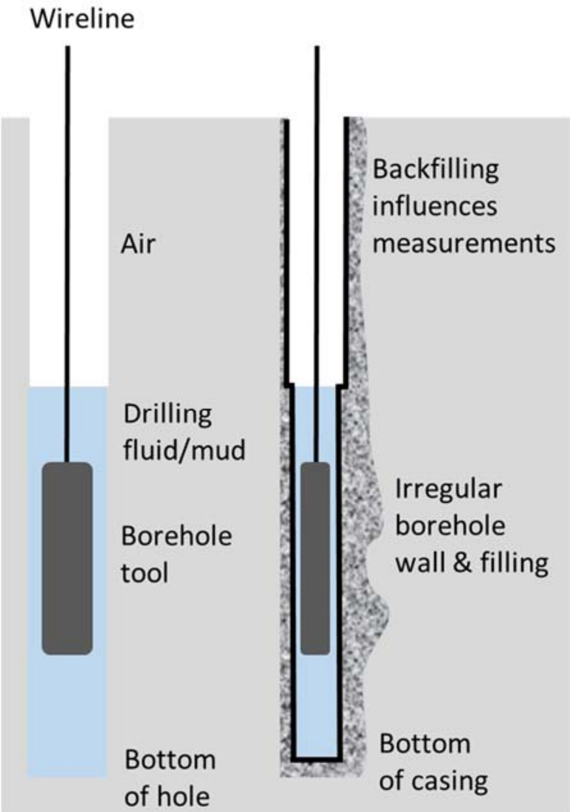


**Figure 1**. Left: ideal logging conditions in a perfect drilled and open hole with a partial water filling. Right: imperfect conditions in a cased hole with a changing diameter and backfilling; modified after Lehmann (2010). Note that sondes are not always centralized, and are tailored to common borehole diameters.

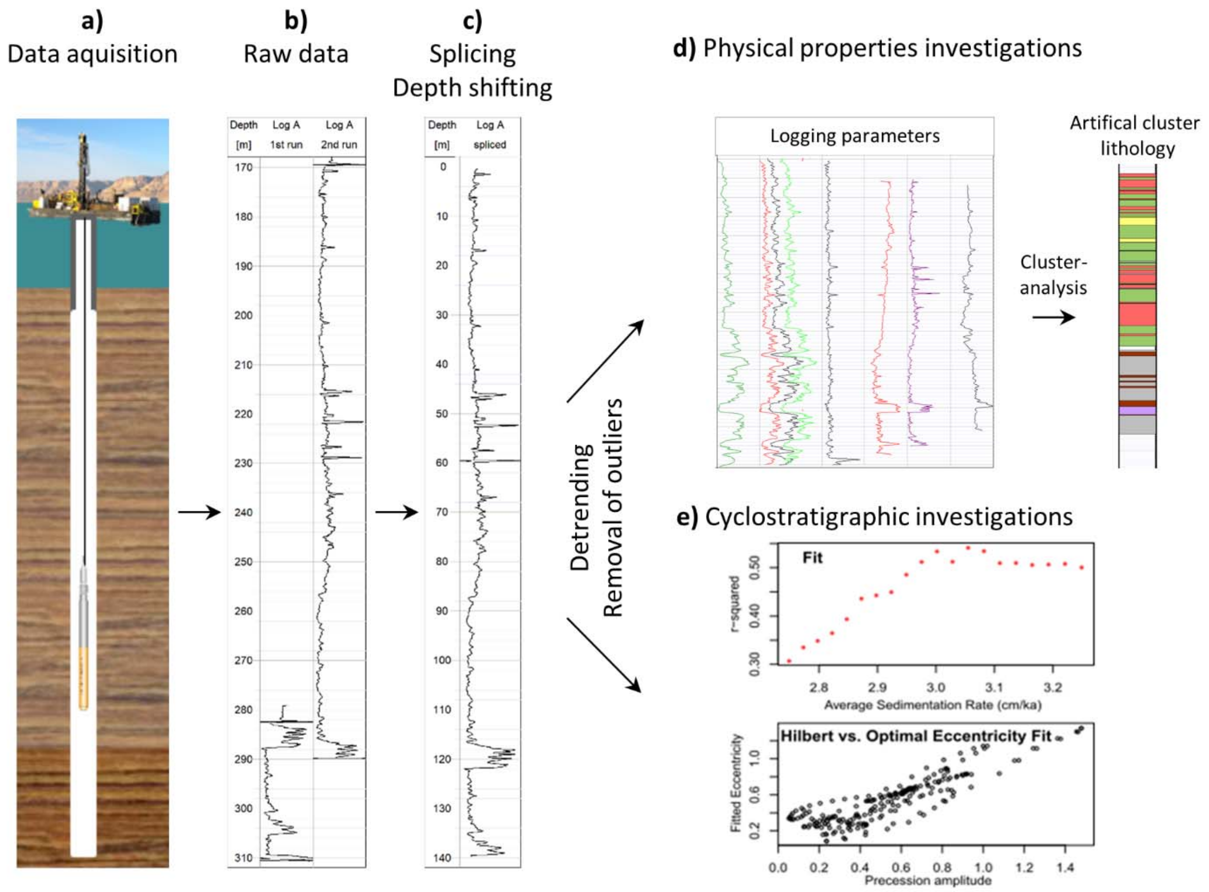


1317

1318 **Figure 2:** Schematic workflow of acquiring and analysing logging data. From left to right: a) data
1319 acquisition, shown here in a lake; b) logging data from two runs; c) spliced logging data. Data analyses
1320 regarding lithology (d), and the time encompassing the dataset (e).

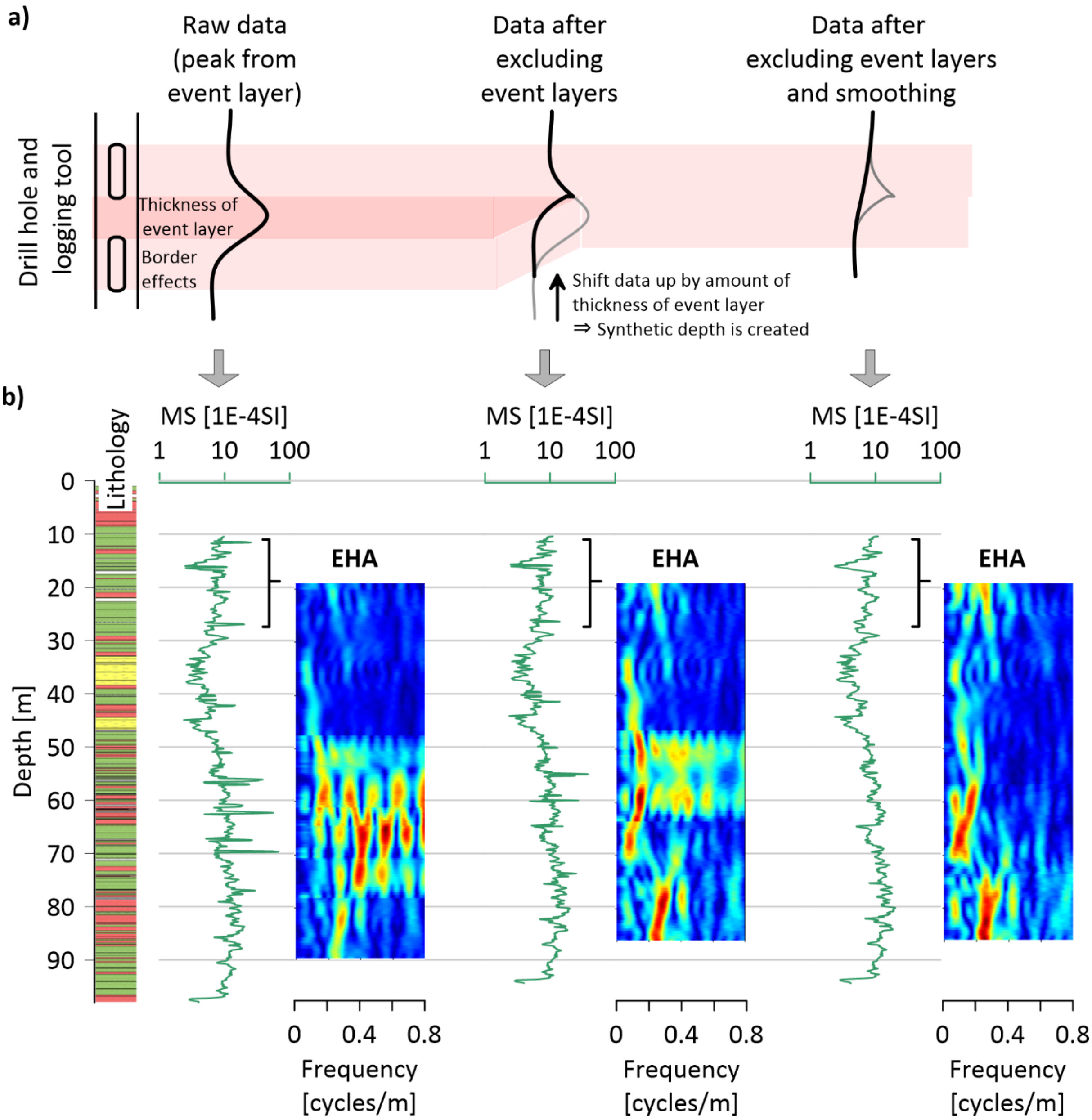


**Figure 3:** Effects of processing downhole logging data on cyclostratigraphic analysis. The upper panel (a) shows the schematic processing steps of removing one event layer. During the borehole measurements, a peak with characteristic border effects arises in the area of the event layer (e.g. tephra, turbidite). When excluding the event layers, the entire record is reduced by the amount of all event layers (thus shortened), but border effects are still present. In the final step, these border effects are smoothed. The lower panel (b) shows these processing steps on real MS data from Lake Towuti (Ulfers et al., 2021). Note the missing 3.5 m on the lower end of the record after the first processing step. Also shown is the effect these processing steps have on evolutive harmonic analysis. Without processing the investigator could be misled by the dominance of the high-frequency signals in the spectrum relating to lithologically clearly different event layers. After processing, the remaining dominant frequencies are in the bandwidth of eccentricity (see Ulfers et al. (2021) for details).

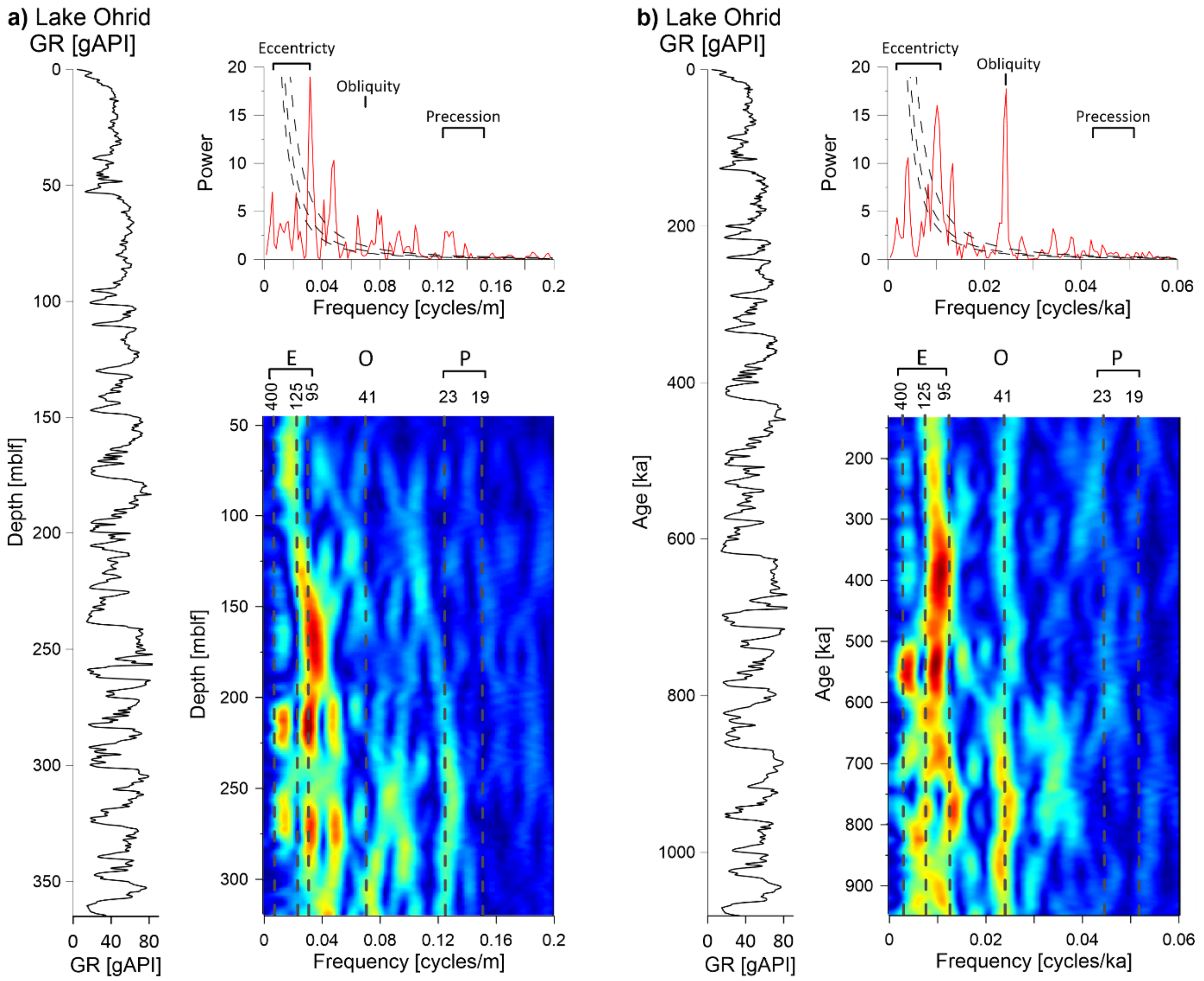


**Figure 4:** This figure shows the differences of 'classic' spectral methods averaging over long depth/time intervals, here power spectra, and time evolutive methods, here evolutive harmonic analyses. In both cases, we investigated the GR record of the last ~ 1 Ma in Lake Ohrid on a) its depth scale and b) in the time domain (Ulfers et al., 2022b). In the power spectrum and in the evolutive analysis in a), the dominant orbital signals appear to be related to eccentricity. However, the position of the orbital components is based on constant average sedimentation rate of 34.4 cm/kyr and may vary over depth (Ulfers et al., 2022b). The power spectrum in b) shows dominant eccentricity and obliquity components. However, it is not possible to make statements about changes in the dominance of a certain component with time. In the evolutive analysis in b), the amplitude of the obliquity signal is substantially reduced after ~600 ka, and the eccentricity component is more dominant in the younger part of the record.

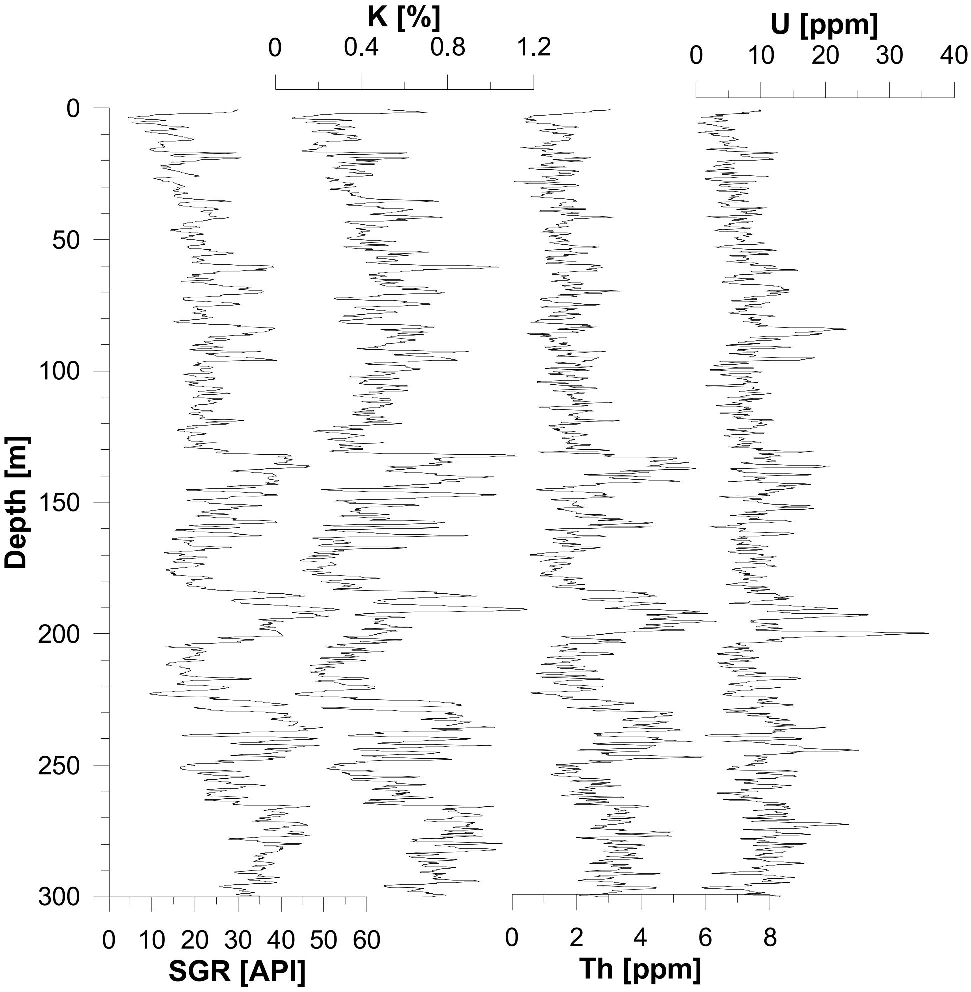


**Figure 5:** Spectral Gamma Ray (SGR, left) from Lake Chalco (Sardar Abadi et al., 2022), and the components from potassium (K), thorium (Th), und uranium (U). Note that while there are similarities between the components, there are differences, which can be used for specific interpretations.

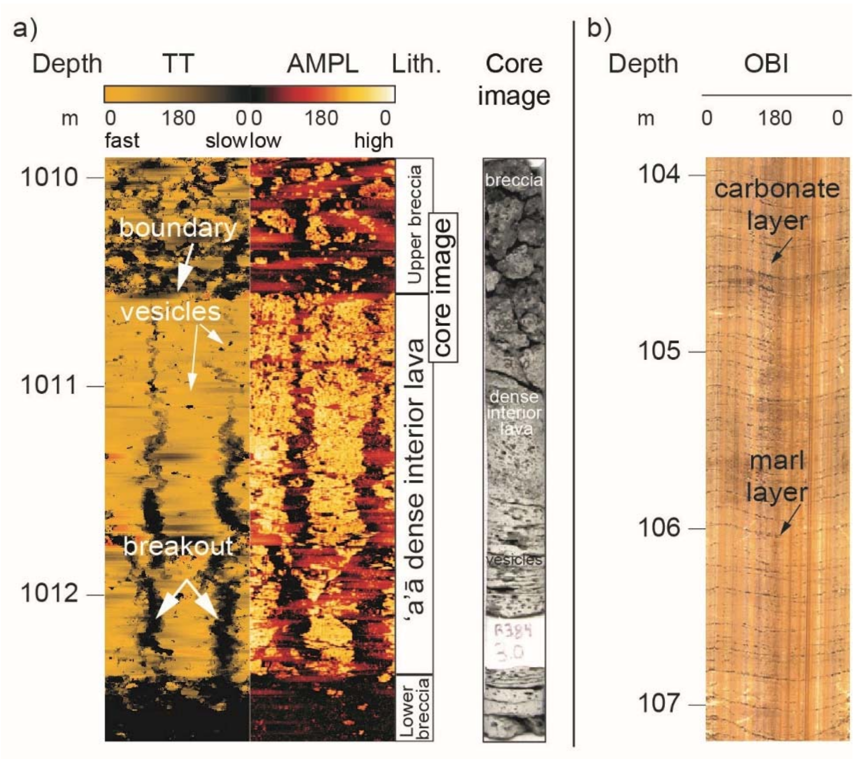


**Figure 6:** An example of acoustic borehole image log and drill core sample from the PTA2 borehole on the island of Hawai'i (modified from Pierdominici et al., 2020). Structural and geological features of an ´a´ā lava facies are shown: lithological change (boundary), vesicles, borehole breakout. The 'a'ā lava flows show instead auto-brecciated upper and lower crusts separated by a vesicular interior. b) An example of an optical borehole image (OBI) from a quasi-cyclic pelagic sedimentary sequence, the Scaglia Rossa in the central Apennines (Italy; e.g., Johnsson and Reynolds, 1986; Turtù et al., 2017). The OBI image shows a rhythmic layering of thick limestone layers (reddish colour) and thin marly intervals (black colours); a paleoclimatic mechanism driven by orbital climate forcing is responsible for the marl-limestone alternation (Johnsson and Reynolds, 1986; Turtù et al., 2017). Legend: TT: travel time; AMPL: amplitude; Lith.: lithology.

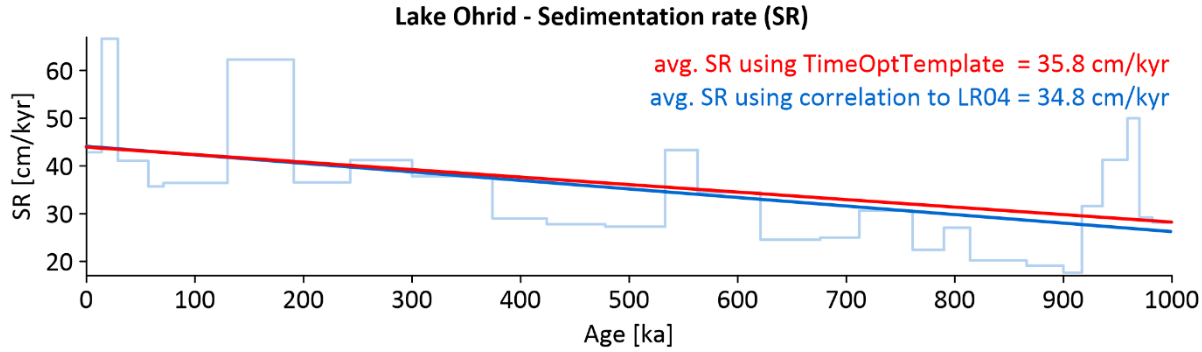


**Figure 7:** Comparison of linear fits through sedimentation rates at the main site in Lake Ohrid using two independent methods. The red line represents results from the timeOptTemplate method (Meyers, 2019, 2015; R Core Team, 2022), while the blue line represents the running average of the sedimentation rate in the background. This in turn is based on a correlation approach using the LR04 benthic stack from Lisiecki and Raymo (2005), and shows the sedimentation rate for each Marine Isotope Stage during the last million years. Both methods are based on GR downhole logging data in Lake Ohrid (see Ulfers et al., 2022b for details on used methods).

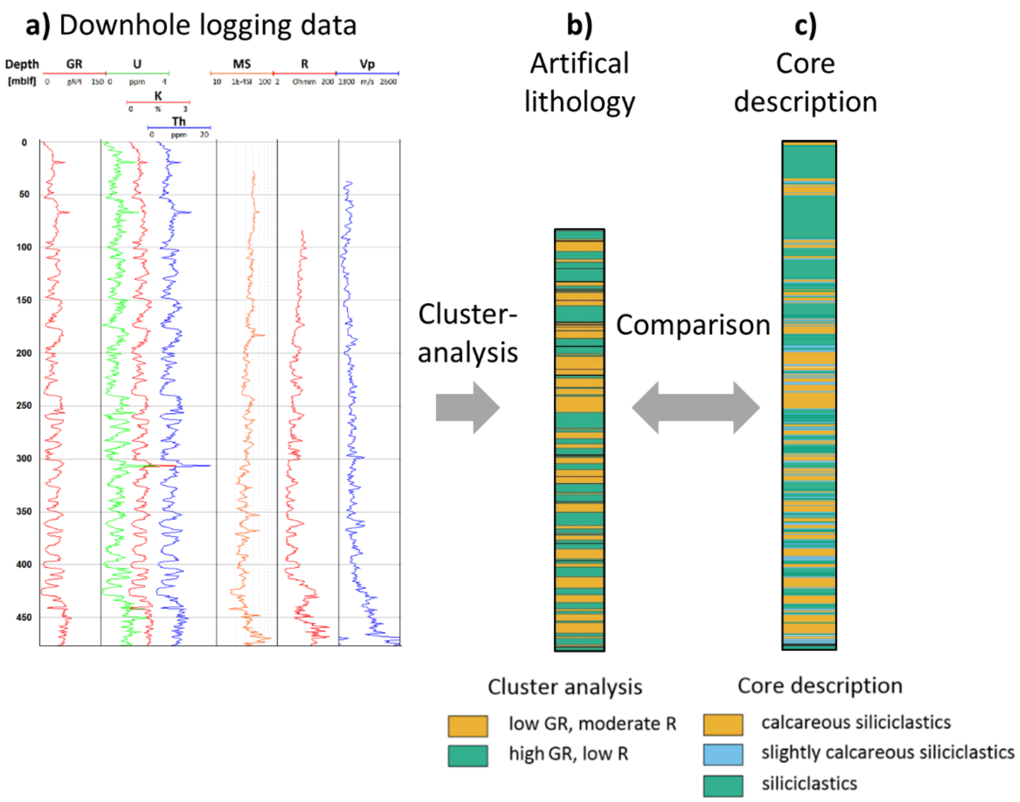


**Figure 8**: Example for cluster analysis using downhole logging data from Lake Ohrid (Baumgarten et al., 2015; Ulfers et al., 2022b). a) shows the logging data which were used for cluster analysis, b) shows the result of cluster analysis from this case, and c) gives a comparison to lithological data (after Ulfers et al., 2022b, adjusted). Note that the results of cluster analysis match the actual core description by (A. Francke et al., 2016; Leicher et al., 2021) well; this is commonly the case. In some cases downhole logging data based cluster analysis is the only way to assess lithology in intervals where cores could not be recovered.